CHEMISTRY OF MATERIALS

Article

pubs.acs.org/cm

Precise Engineering of Multifunctional PEGylated Polyester Nanoparticles for Cancer Cell Targeting and Imaging

Nicolas Mackiewicz,[†] Julien Nicolas,*[,†] Nadège Handké,[†] Magali Noiray,[†] Julie Mougin,[†] Cyril Daveu,[‡] Harivardhan Reddy Lakkireddy,[§] Didier Bazile,[§] and Patrick Couvreur[†]

[†]Institut Galien Paris-Sud, Univ Paris-Sud, UMR CNRS 8612, Faculté de Pharmacie, 5 rue Jean-Baptiste Clément, F-92296 Châtenay-Malabry cedex, France

[‡]Sanofi Research and Development, Fibrosis and Wound Repair, 1 avenue Pierre Brosselette, F-91385 Chilly-Mazarin cedex, France

[§]Sanofi Research and Development, Lead Generation to Candidate Realization Platform, 13 quai Jules Guesde, F-94403 Vitry-sur-Seine cedex, France

Supporting Information

ABSTRACT: Multifunctional poly(ethylene glycol)-*block*-poly(lactic acid) (PEG-*b*-PLA) nanoparticles for cancer cell targeting and imaging have been designed by a combination of ring-opening polymerization and "click" chemistry. Nanoparticles containing both a targeting ligand and a fluorescent probe were prepared by blending PLA-*b*-PEG−ligand, PLA-*b*-PEG−fluorescent probe, and PLA-*b*-PEG−OMe copolymers at the molar ratios necessary to achieve the desired surface ligand and fluorescent probe densities. This strategy has been illustrated by the preparation of a large library of a variety of nanoparticles, such as ligand-decorated nanoparticles (with biotin, folic acid or anisamide), fluorescent nanoparticles (UV−vis or near-infrared dyes), and multifunctional nanoparticles decorated with a targeting ligand and a fluorescent probe. Successful targeting was demonstrated by surface plasmon resonance and in vitro experiments on different cancer cell lines.

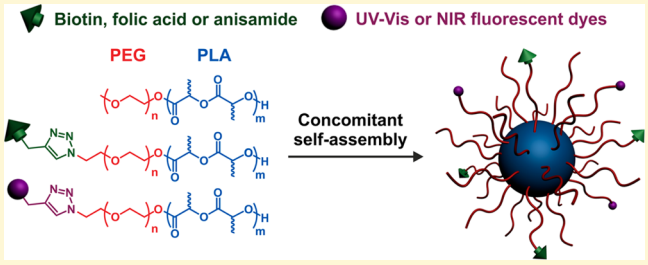

INTRODUCTION

Spurred by the development of advanced nanoscale systems for drug delivery, the field of nanomedicine has recently received tremendous attention.[1,2] Since many drugs exhibit a low therapeutic efficacy due to nonspecific tissue distribution, as well as to rapid metabolism and/or excretion from the body, their encapsulation into colloidal nanocarriers, able to ensure a safe transport from the injection site to the therapeutic target, has been widely investigated.[3−6] The efficacy and safety of therapeutic drugs depends on the ability to deliver those to the target disease sites with a minimal distribution to off-target organs of the body. When the drugs reach the target organ, only those drugs possessing the ability to penetrate into the target cells show efficacy. However, the drugs possessing poor cell penetration remain inactive because their intracellular access remains poor, even if they are delivered efficiently to the extracellular space of the target organ. For such drugs, the use of intelligent approaches to enhance their intracellular delivery is a key requisite for enhancing their therapeutic efficacy, for instance through the design of targeted[7−9] or stimuli-responsive nanoparticulate systems.[10] Among the different classes of carrier materials suitable for the development of nanomedicines, biodegradable polymers perhaps represent the best candidates due to the flexibility and robustness offered by macromolecular synthesis methods, the great diversity of macromolecular architectures, and their ease of functionalization.[11] However, examples of polymeric nanoparticulate systems gathering all prerequisites for targeted drug delivery (i.e., biodegradable, stealth, traceable, and targeted) are rather scarce, thus deserving more research effort in this area.

In this context, nanoparticles made of polyesters, such as poly(lactic acid) (PLA) or poly(lactic-*co*-glycolic acid) (PLGA), hold great promise in the field, due to their biocompatibility and biodegradability,[12,13] and are Food and Drug Administration-approved polymers. The vast majority of functionalized polyester nanoparticles with surface-installed recognition ligands, or functional groups for subsequent coupling with biologically active ligands, are generally obtained by carbodiimide-assisted coupling chemistry or Michael addition, using naturally occurring terminal groups (e.g., COOH, NH_2, OH) of polyester chains (or PEG for PEGylated nanoparticles).[7] Although very convincing examples of active targeting using polyester nanoparticles have been reported by such functionalization pathways,[14−20] noteworthy is the fact that most of these systems face substantial lack of both flexibility regarding the nanoparticle functionalization (i.e., difficulty to tune/control the amount of exposed ligand when the functionalization is achieved on preformed nanoparticles) and

Received: November 18, 2013
Revised: February 4, 2014
Published: February 5, 2014

   dx.doi.org/10.1021/cm403822w | *Chem. Mater.* 2014, 26, 1834−1847

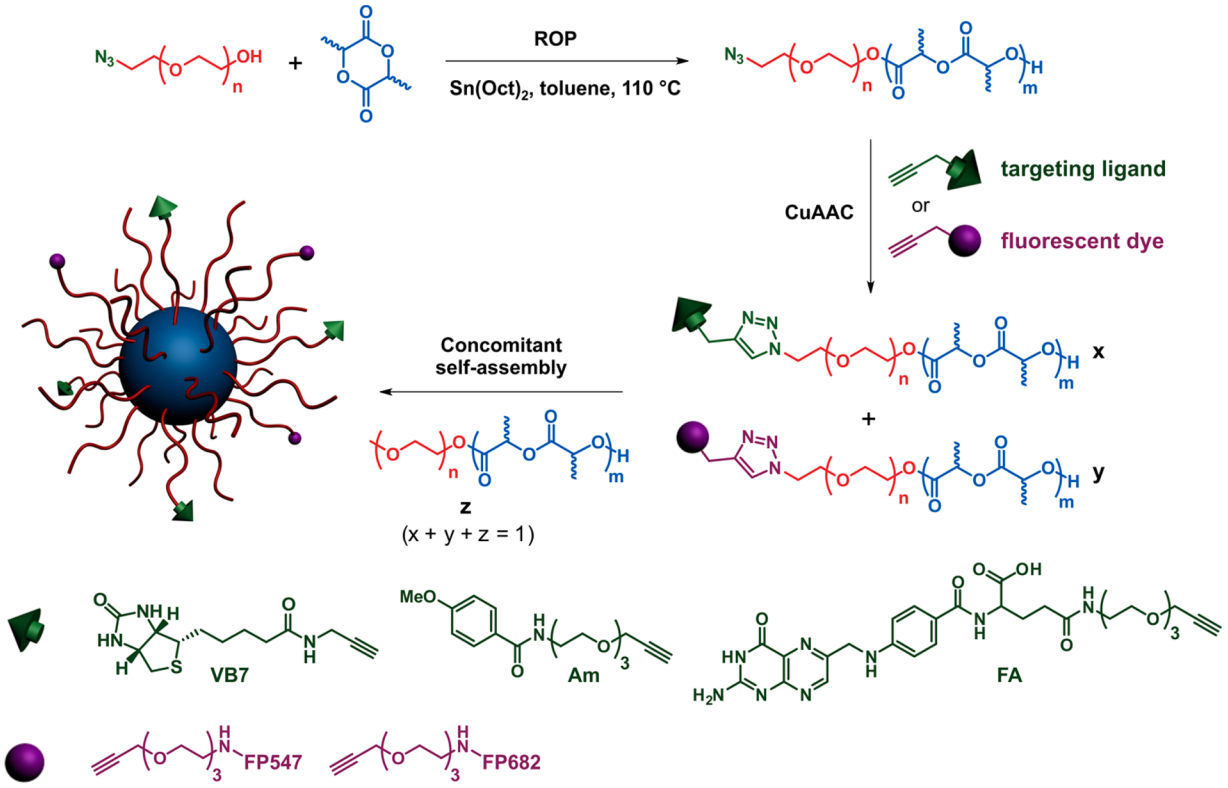

Figure 1. Synthetic pathway to prepare tunable targeted and fluorescent PEGylated polylactide nanoparticles by a combination of ring-opening polymerization (ROP), copper-catalyzed azide−alkyne cycloaddition (CuAAC), and concomitant self-assembly into nanoparticles in aqueous solution. Targeting ligands: biotin (VB7), anisamide (Am), and folic acid (FA). Fluorescent ligands: FP547 and FP682.

diversity regarding the nature of the exposed ligands (i.e., a customized synthetic pathway is usually required for each ligand). In addition, biologically active ligands are likely to bear multiple functional groups that can be sensitive to carbodiimide chemistry, leading to side reactions and/or multisite attachments unless additional steps of protection/deprotection are undertaken. Copper-catalyzed azide−alkyne Huisgen 1,3-dipolar cycloaddition (CuAAC), often termed "click" chemistry, may then offer valuable benefits in the sense of its exceptional efficiency and selectivity under relatively mild conditions.[21,22] CuAAC has indeed received tremendous interest as an established synthetic route to obtain tailor-made complex materials and has been exploited in many research areas, among them being dendrimers,[23−25] bioconjugates,[26−28] therapeutics,[29−31] and functionalized polymers.[32−36] However, very few examples of surface-functionalized PEGylated biodegradable nanoparticles by click chemistry have been reported so far.[37−41] For instance, in the case of polyester nanoparticles, Alexander and co-workers elegantly reported biologically active folic acid (FA)-functionalized PLGA-*b*-poly(oligoethylene glycol methyl ether methacryate) block copolymer nanoparticles for gene delivery, whose FA moiety was "clicked" at the extremity of the polymethacrylate backbone.[40] FA has also been clicked at the surface of azido-decorated PLA-*b*-PEG nanoparticles, but no targeting evaluation has been reported.[39]

In order to tackle the above-mentioned issues, we report here a general strategy deriving from well-established long-circulating PLA-*b*-PEG amphiphilic block copolymer nanoparticles[42,43] to furnish multifunctional nanoparticles with tunable dual click functionalization with both imaging probes and various targeting ligands for theranostic purposes (Figure 1). Therefore, the nanoparticles comprise (i) a biodegradable core made of PLA, (ii) a PEG shell for improved colloidal stability and stealth features,[42] and (iii) surface-displayed biologically active ligands for cancer cell targeting and fluorescent dyes for imaging/tracing purposes, both tethered by CuAAC at the distal end of the PEG chains. The idea was to synthesize a "clickable" PLA-*b*-PEG−N_3 copolymer, which is further reacted via CuAAC with the desired alkyne derivative (Figure 1).[44] Therefore, by adjusting the stoichiometry of a blend comprising PLA-*b*-PEG−ligand and other copolymers (functionalized or not), tunable multifunctional nanoparticles can be readily prepared by concomitant self-assembly in aqueous solution. The robustness of our approach is illustrated by the derivatization of the PEGylated nanoparticles with a library of ligands. For cancer cell targeting, we used anisamide (Am), which possesses high affinity for σ-receptors,[45,46] and two vitamins, folic acid (FA) and biotin (VB7), that respectively recognize folate and biotin receptors, overexpressed at the surface of many cancer cells.[38,47,48] For imaging purposes, we used two hemicyanine dyes, FP547 and FP682, which emit in the UV−vis region and in the near-infrared (NIR) suitable for in vivo imaging, respectively. This approach is expected to open interesting prospects for targeted drug delivery and theranostic applications.

EXPERIMENTAL SECTION

1. Materials. Methoxypoly(ethylene glycol), stannous octoate [$Sn(Oct)_2$], anhydrous toluene, dimethylaminopyridine (DMAP), triethylamine (TEA), methanesulfonyl chloride (MsCl), sodium azide (NaN_3), magnesium sulfate ($MgSO_4$), concentrated hydrochloric acid (conc HCl), sodium hydroxide (NaOH), *N*-bromosuccinimide (NBS), triphenyl phosphine (PPh_3), hydrobromic acid (HBr), triethylene glycol, sodium hydride (NaH), propargyl bromide, potassium

dx.doi.org/10.1021/cm403822w | *Chem. Mater.* 2014, 26, 1834−1847

phthalate, sodium iodide, methanesulfonyl chloride, hydrazine hydrate, *N*-(3-dimethylaminopropyl)-*N*′-ethylcarbodiimide hydrochloride (EDC), *N*-hydroxysuccinimide (NHS), folic acid, (benzotriazol-1-yloxy)tripyrrolidinophosphonium hexafluorophosphate (PyBOP), *p*-methoxybenzoic acid, *N*,*N*-diisopropylethylamine (DIEA), copper bromide (CuBr), *N*,*N*,*N*′,*N*″,*N*″-pentamethyldiethylenetriamine, (PMDETA), Pluronic F68, sodium bicarbonate, and DMEM 2429 were purchased from Sigma-Aldrich (Saint-Quentin Fallavier, France) and used as received. D,L-Lactide (Biovalley) was recrystallized from ethyl acetate twice and then dried under vacuum. FP547−NHS and FP682−NHS were purchased from Interchim (Montluçon, France). PEG_{2500}-benzyl was purchased from Polymer Source Inc. (Quebec, Canada). Penicillin, fetal bovine serum (FBS), phosphate-buffered saline (PBS), and L-glutamine were purchased from Lonza (Levallois, France). Trypsin EDTA was purchased from Invitrogen Gibco (Saint-Aubin, France). DMEM and RPMI1640 were purchased from Fisher Scientific (Illkirch, France). 3-(4,5-Dimethylthiazol-2-yl)-5-(3-carboxymethoxyphenyl)-2-(4-sulfophenyl)-2*H*-tetrazolium (MTS), a tetrazolium compound included in the CellTiter 96 AQ_{ueous} Non-Radioactive Cell Proliferation Assay, was purchased from Promega (Lyon, France). All common solvents were used as received without further distillation and were purchased from Carlo Erba. Alkynated biotin (VB7−alkyne) was prepared as published elsewhere.[38,49]

2. Synthetic Pathways. *2.1. Synthesis of PLA-b-PEG−OMe Copolymer (**C1**).* To a mixture of methoxypoly(ethylene glycol) ($M_{n,NMR}$ = 2010 g·mol^{-1}, 245 mg, 0.12 mmol) and D,L-lactide (7.01 g, 48.62 mmol) was added, under dry conditions, a solution of $Sn(Oct)_2$ (18.7 mg, 46.1 μmol) in anhydrous toluene (11.2 mL). The reaction mixture was degassed by bubbling argon for 20 min and then stirred in a preheated oil bath at 120 °C for 30 min under inert atmosphere. The reaction was stopped at approximately 54% of monomer conversion. The toluene was removed under reduced pressure and the obtained product was dissolved into a minimum amount of dichloromethane (DCM) and further precipitated in diethyl ether (Et_2O). The precipitate was then dissolved into a minimum amount of tetrahydrofuran (THF) and further precipitated in water and subsequently freeze-dried overnight to yield a white powder ($M_{n,NMR}$ = 33 200 g·mol^{-1}, $M_{n,SEC}$ = 26 100 g·mol^{-1}, $Đ$ = 1.14). ^{1}H NMR (400 MHz, $CDCl_3$, δ in ppm): 5.34−4.85 (m, 434H), 4.40−4.17 (m, 3H), 3.86−3.41 (m, 186H), 3.36 (s, 3H), 1.77−1.19 (m, 1302H).

*2.2. Synthesis of PLA-b-PEG−N_3 (**C2**). Synthesis of Bz−PEG−N_3.* To a solution of PEG_{2500}-benzyl ($M_{n,NMR}$ = 2570 g·mol^{-1}, 2.43 g, 0.94 mmol, 1 equiv), DMAP (58 mg, 0.5 equiv), and TEA (747 μL, 5.6 equiv) in DCM (65 mL), cooled to 0 °C, is slowly added MsCl (326 μL, 4.4 equiv) over 20 min (*Caution: Note that MsCl is highly reactive and corrosive and therefore should be handle with great care*). The reaction was stirred overnight at room temperature and concentrated under reduced pressure. The residue was dissolved into dimethylformamide (DMF, 20 mL) and to it was added sodium azide (330 mg, 5.3 equiv). The reaction mixture was stirred at 50 °C for 24 h and concentrated under reduced pressure, and the residue was dissolved into 50 mL of brine and subsequently washed three times with the same volume of brine. The organic layer was dried over $MgSO_4$, filtered, and concentrated under reduced pressure to a minimum volume of DCM. The latter was precipitated into Et_2O to give a white powder (2.16 g, 88% yield). ^{1}H NMR (300 MHz, $CDCl_3$, δ in ppm): 7.30−7.05 (m, 5H), 4.43 (s, 2H), 3.93−3.03 (m, 222H), 3.27 (t, 2H).

Synthesis of HO−PEG−N_3. Bz−PEG−N_3 (2.16 g, 0.83 mmol, 1 equiv) was solubilized into conc HCl (20 mL) and stirred at room temperature for 2 days. A solution of concentrated NaOH was added up to pH 1.0. The aqueous phase was extracted with DCM (four times with 50 mL), and the combined organic layers were dried over $MgSO_4$, filtered, and concentrated under reduced pressure to a minimum volume of DCM. The latter was precipitated into Et_2O to give a white powder (1.89 g, 91% yield). $M_{n,NMR}$ = 2510 g·mol^{-1}. ^{1}H NMR (400 MHz, $CDCl_3$, δ in ppm): 3.73−3.33 (m, 222H), 3.27 (t, J = 5.0 Hz, 2H), 2.75 (s, 1H).

Synthesis of PLA-b-PEG−N_3. A typical synthesis is as follows. To a mixture of HO−PEG−N_3 (293 mg, 0.12 mmol) and D,L-lactide (7.01 g, 48.62 mmol) was added, under dry conditions, a solution of $Sn(Oct)_2$ (18.7 mg, 46.1 μmol) in anhydrous toluene (11.2 mL). The reaction mixture was degassed by bubbling argon for 20 min and then stirred in a preheated oil bath at 120 °C for 90 min under inert atmosphere. The reaction was stopped at approximately 55% of monomer conversion. Toluene was removed under reduced pressure, and the obtained product was dissolved into a minimum volume of DCM and subsequently precipitated in Et_2O. The precipitate was then dissolved into a minimum amount of THF, further precipitated in water, and subsequently freeze-dried overnight to yield a white powder. ($M_{n,NMR}$ = 29 200 g·mol^{-1}, $M_{n,SEC}$ = 20 100 g·mol^{-1}, $Đ$ = 1.11). ^{1}H NMR (400 MHz, $CDCl_3$, δ in ppm): 5.41−4.83 (m, 377H), 4.38−4.15 (m, 3H), 3.84−3.40 (m, 222H), 3.36 (t, J = 4.8 Hz, 2H), 1.82−1.21 (m, 1132H).

2.3. Synthesis of the Amino−Tri(ethylene glycol)−Alkyne (H_2N−TEG−Alkyne) Linker. Synthesis of Monoalkyne Triethylene Glycol. Triethylene glycol (5.62 g, 37.4 mmol, 1 equiv) was dissolved in anhydrous THF (50 mL) and the resulting solution was cooled to 0 °C under dry conditions. Sodium hydride (0.99 mg, 1.1 equiv) was added slowly to the above solution followed by dropwise addition of propargyl bromide (80 wt % in toluene, 4.36 mL, 1.1 equiv). The reaction mixture was stirred for 12 h at room temperature under inert atmosphere. THF was removed under reduced pressure, and the residue was taken into DCM and washed several times with brine. The resulting organic layer was dried over $MgSO_4$, filtered, concentrated under reduced pressure, and dried under vacuum. The crude product was purified by column chromatography over silica [cyclohexane (cHex)/ethyl acetate (AcOEt) 8/2] to give a yellow oil (3.31 g, 47% yield). ^{1}H NMR (300 MHz, $CDCl_3$, δ in ppm): 4.15 (d, J = 2.4 Hz, 2H), 3.70−3.60 (m, 10H), 3.57−3.53 (m, 2H), 2.70 (m, 1H), 2.41 (t, J = 2.4 Hz, 1H).

Synthesis of Phthalimide−Monoalkyne Triethylene Glycol. To a solution of monoalkyne triethylene glycol (4.0 g, 212 mmol, 1 equiv) in DCM (60 mL) was added, dropwise under inert atmosphere, a catalytic amount of DMAP, MsCl (3.3 mL, 2 equiv), and TEA (5.9 mL, 2 equiv). The reaction mixture was stirred for 4 h at room temperature. The solution was washed with brine (three times with 50 mL), the aqueous phase was then extracted with DCM (50 mL), and the combined organic layers were dried over $MgSO_4$, filtered, and concentrated under reduced pressure. To the previous preparation (5.1 g, 19.2 mmol, 1 equiv) dissolved in DMF (100 mL) was added potassium phthalate (7.87 g, 2.2 equiv) and a catalytic amount of sodium iodide (less than 1 equiv, e.g., a spatula tip). The solution was stirred at 80 °C overnight and the solvent was removed under reduced pressure. The resulting residue was purified by column chromatography over silica (cHex/AcOEt; from 2/8 to 4/6) to give a yellow oil (5.7 g, 94% yield). ^{1}H NMR (300 MHz, $CDCl_3$, δ in ppm): 7.81 (dd, J = 5.5, 3.0 Hz, 2H), 7.69 (dd, J = 5.5, 3.0 Hz, 2H), 4.13 (d, J = 2.4 Hz, 2H), 3.80 (dt, J = 11.4, 6.0 Hz, 4H), 3.65 − 3.56 (m, 8H), 2.40 (t, J = 2.4 Hz, 1H).

Synthesis of H_2N−TEG−Alkyne. Phthalimide−alkyne triethylene glycol (2.03 g, 6.4 mmol, 1 equiv) was dissolved in ethanol (EtOH, 200 mL) and to this solution was added hydrazine hydrate (3.1 mL, 10 equiv). The reaction mixture was stirred overnight under reflux conditions. The reaction was cooled to room temperature and 8 mL of conc HCl was added to the reaction mixture (pH ∼2−3). The precipitate was removed by filtration and the pH was raised to above 10 using 2 M NaOH solution. The aqueous phase was extracted three times with DCM, and the resulting organic layer was dried over $MgSO_4$, filtered, concentrated under reduced pressure, and dried under vacuum; 911 mg of yellow oil was recovered (76% yield). ^{1}H NMR (300 MHz, $CDCl_3$, δ in ppm): 4.13 (d, J = 2.4 Hz, 2H), 3.69−3.50 (m, 8H), 3.43 (t, J = 5.2 Hz, 2H), 2.79 (t, J = 5.2 Hz, 2H), 2.38 (t, J = 2.4 Hz, 1H), 1.33 (s, 2H). ^{13}C NMR (75 MHz, $CDCl_3$, δ in ppm): 79.64, 74.53, 73.47, 70.59, 70.40, 70.25, 69.09, 58.37, 41.80.

2.4. Synthesis of Alkynated Ligands. Synthesis of Folic Acid−Alkyne Triethylene Glycol (FA−TEG−Alkyne). To a solution of amino alkyne triethylene glycol (319 mg, 1.70 mmol, 1 equiv) in DMF (70 mL) was added, under inert atmosphere, EDC (393 mg, 1.2 equiv), NHS (236 mg, 1.2 equiv), and few drops of TEA. The reaction was heated up to 50 °C and folic acid (754 mg, 1 equiv) was added to the reaction mixture. The reaction was then stirred overnight at 50 °C.

The solution was concentrated under reduced pressure. The residue was precipitated into a mixture of DCM and acetone, filtered, and dried under vacuum. The alkyne−FA conjugate γ-isomer (biologically more active)[50,51] was purified by preparative HPLC in order to remove unreacted FA, dialkyne FA, and the α-isomer (biologically less active). The HPLC purification consisted of a reverse-phase column (C18, Kromasil 10 μm, 4.6 × 250 mm) using a 5−95% acetonitrile gradient in 20 mM ammonium acetate buffer (adjusted to pH 5) for 20 min followed by 95% acetonitrile for 5 min. The product was then solubilized in 20% DMF in the eluent. Further purification was carried out on Kromasil C18 10 μm packed in a 100 mm column (1.5 kg of phase) eluting with a 20 mM 85% ammonium acetate buffer (pH 5) and 15% acetonitrile; 200 mg of raw product was eluted at the same time as the DMF injection peak. The final purification was performed using preparative HPLC with a reverse-phase column (Waters XBridge 30 × 100, 5 μm) by dissolving 200 mg of the raw product in DMSO (5 mL) and subsequently adding 5 mL of buffer solution (10 mM ammonium carbonate adjusted to pH 9.3 with a 28% aqueous ammonia solution) to it. Ten injections of 1 mL were performed using a gradient going from 95:5 (buffer solution ammonium carbonate/acetonitrile) to 5:95 in 12 min at 30 mL·min^{-1}. ^{1}H NMR (400 MHz, DMSO-d_6, δ in ppm): 8.61 (s, 1H), 8.29 (br, 1H), 7.8 (t, J = 6.1 Hz, 1H), 7.67 (d, J = 8.2 Hz, 2H), 7.03 (br, 2H), 6.85 (t, 1H), 6.62 (d, J = 8.2 Hz, 2H), 4.44 (d, J = 6.5 Hz, 2H), 4.31 (q, J = 5.1, 8.2 Hz, 1H), 4.12 (d, J = 2.2 Hz, 2H), 3.57−3.36 (m, 12H), 3.50 (hidden t, 1H), 3.35−3.1 (hidden m, 2H), 2.23 (t, J = 7.2 Hz, 2H), 1.91 (dquint, 2H). LCMS: 611 $[M + H]^+$.

Synthesis of Anisamide−Alkyne Triethylene Glycol (Am−TEG−Alkyne). To a solution of amino alkyne triethylene glycol (200 mg, 1.07 mmol, 1 equiv) in DCM (20 mL) was added, under inert atmosphere, PyBOP (780 mg, 1.4 equiv), *p*-methoxybenzoic acid (229 mg, 1.4 equiv), and DIEA (260 μL, 1.4 equiv). The reaction mixture was stirred overnight at room temperature. The solution was washed with brine (three times with 20 mL) and the aqueous phase was extracted with DCM (20 mL). The combined organic layers were dried over $MgSO_4$, filtered, and concentrated under reduced pressure. The crude product was purified by column chromatography over silica (eluent cHex/AcOEt 5/5 to 7/3) to give a yellow oil (300 mg, 90% yield). ^{1}H NMR (300 MHz, $CDCl_3$, δ in ppm): 7.74 (d, J = 8.8 Hz, 2H), 6.87 (d, J = 8.9 Hz, 2H), 6.84 (br, 1H), 4.14 (d, J = 2.4 Hz, 2H), 3.81 (s, 3H), 3.71−3.53 (m, 12H), 2.42 (t, J = 2.4 Hz, 1H).

Synthesis of FP547−Alkyne Triethylene Glycol (FP547−TEG−Alkyne) and FP682−Alkyne Triethylene Glycol (FP682−TEG−Alkyne). To a solution of FP547−NHS (2.5 mg, 2.55 μmol, 1 equiv) in DMSO (356 μL) was added a solution of DMSO (92 μL) containing EDC (0.49 mg, 1 equiv), NHS (0.29, 1 equiv), TEA (0.35 μL, 1 equiv), and amino alkyne triethylene glycol (1.07 mg, 2.2 equiv). The mixture was stirred in the dark at room temperature for 12 h. The reaction mixture was concentrated under reduced pressure, dissolved into DCM, and extracted with brine. A pink oil was obtained, which was subsequently characterized using UV/vis, fluorescence spectroscopy, and ^{1}H NMR. The resulting spectra were found to be similar to those provided by the supplier of the fluorophore compound. The same protocol was used for the synthesis of FP682−TEG−alkyne.

2.5. Conjugation of Alkynated Ligands to PLA-b-PEG-N_3 Copolymer. A representative synthesis (PLA-*b*-PEG−Am, **C4**) was as follows (note that molar equivalents of reactants are identical from one conjugation experiment to another). To a degassed solution of PLA-*b*-PEG−N_3 (**C2**, 200 mg, 5.52 μmol, 1 equiv) and alkyne anisamide (32 mg, 0.1 mmol, 18 equiv) in anhydrous DMF (6 mL) was added, with a syringe, a degassed solution of CuBr (5.5 mg, 6.9 equiv) and PMDETA (20 μL, 17 equiv) in anhydrous DMF (400 μL). The reaction mixture was stirred for 15 h at 40 °C under nitrogen. The solution was concentrated under reduced pressure and the residue was dissolved into a minimum amount of THF and subsequently precipitated in water. The precipitate was freeze-dried, dissolved again into a minimum amount of THF, and further precipitated in water. The precipitate was freeze-dried to yield a white powder. For poorly water-soluble alkyne derivatives (i.e., FA and Am), the first freeze-dried precipitate was dissolved into a minimum volume of DCM and then precipitated in Et_2O. Finally, the precipitate obtained was dissolved in a minimum volume of THF, precipitated into water, and dried under high vacuum until constant weight. By ^{1}H NMR, the coupling yield was determined to be 90% (integration of the peaks at 6.95 and 7.8 ppm and compared to the signal of PEG at 3.2 ppm). The same methodology was also applied to alkynated folic acid (16.3 equiv, 50 °C, 15 h, coupling yield = 76%; integration of the peaks at 6.65, 7.65, and 8.65) to obtain PLA-*b*-PEG−FA (**C3**), to alkynated FP547 [0.3 equiv, 50 °C, 15 h, coupling yield = not determined (nd)] to obtain PLA-*b*-PEG−FP547 (**C5**), to alkynated FP682 (0.5 equiv, 40 °C, 18 h, coupling yield = nd) to obtain PLA-*b*-PEG−FP682 (**C6**), and to alkynated VB7 (18 equiv, 50 °C, 24 h, coupling yield = 52%, integration of the peak relative to the triazole proton at 7.86 ppm) to obtain PLA-*b*-PEG−VB7 (**C7**). Another batch of PLA-*b*-PEG−VB7 copolymer (**C8**) pushed on to 76 mol % coupling (reaction twice as long) was further used for SPR experiments.

3. Analytical Techniques. *3.1. Nuclear Magnetic Resonance (NMR) Spectroscopy.* NMR spectroscopy was performed in 5 mm diameter tubes in $CDCl_3$ or DMSO-d_6 at 25 °C. ^{1}H and ^{13}C NMR spectroscopy was performed on a Bruker Avance 300 spectrometer at 300 MHz (^{1}H) or 75 MHz (^{13}C) and a Bruker Avance 400 spectrometer at 400 MHz. The chemical shift scale was calibrated on the basis of the solvent peak.

3.2. Size Exclusion Chromatography (SEC). SEC was performed at 30 °C with two columns from Polymer Laboratories (PL-gel MIXED-D; 300 × 7.5 mm; bead diameter 5 mm; linear part 400 to 4 × 10^5 g·mol^{-1}) and a differential refractive index detector (SpectraSystem RI-150 from Thermo Electron Corp.). Chloroform was used as an eluent at a flow rate of 1 mL·min^{-1} and toluene was used as a flow-rate marker. The calibration curve was based on poly(methyl methacrylate) (PMMA) standards (peak molar masses, M_p = 625−625 500 g·mol^{-1}) from Polymer Laboratories. This technique allowed M_n (the number-average molar mass), M_w (the weight-average molar mass), and M_w/M_n (the dispersity, D) to be determined.

3.3. Dynamic Light Scattering (DLS) and Zeta Potential. Measurement of the nanoparticle diameter (D_z) and the surface charge reported as zeta potential (ζ) was performed using a Nano ZS from Malvern (173° scattering angle) at 25 °C. The particle size distribution values, ranging from 0 to 1, are given by the DLS apparatus and correspond to the ratio of the variance over the square of the average particle diameter. The ζ-potential (mV) measurement was performed after dilution with 1 mM NaCl, using the Smoluchowski equation.

3.4. Transmission Electron Microscopy (TEM). Five microliters of NP dispersion at 10 mg·mL^{-1} was deposed on Formvar/carbon coated grids (400 mesh). After 5 min at room temperature, a drop of phosphotungstic acid 2% filtered on 0.22 μm was added for negative staining and the excess of volume was eliminated. The grids were then observed with a JEOL 1400 120 kV electron microscope operating at 80 kV at a nominal magnification of 5000−40 000. Digital images were directly recorded on a CCD postcolumn high-resolution (11 MegaPixel) high-speed camera (SC1000 Orius, Gatan Inc.) using Digital Micrograph image acquisition and processing software (Gatan Inc.).

4. Nanoparticle Formation. The copolymer or a blend of different copolymers (30 mg in total) was dissolved in AcOEt (1.2 mL). The above organic phase was added to 3.3 mL of an aqueous phase containing 1% w/v Pluronic F68. The mixture was then vigorously shaken using a vortex shaker for 1 min. The resulting emulsion was ultrasonicated (using an ultrasonic probe) for 3 min and the organic solvent was removed under reduced pressure using a rotary evaporator. The resulting nanoparticle suspension was ultracentrifuged at 30 000*g* for 30 min and the pellet was resuspended in 3 mL of pH 7.4 PBS. The nanoparticles were filtered through a 1 μm glass filter disk (Acrodisc) and stored at 4 °C until use.

5. Cell Culture. KB-3-1 cells originating from human cervix carcinoma, were obtained from Pr. S. Chevillard. These cells were cultured in monolayers in two different media in order to induce or not an overexpression of the folate receptors, supplemented with 1% penicillin/streptomycin and 10% v/v FBS in a 5% CO_2 humidified atmosphere at 37 °C. The medium used to overexpress the folate

dx.doi.org/10.1021/cm403822w | *Chem. Mater.* 2014, 26, 1834−1847

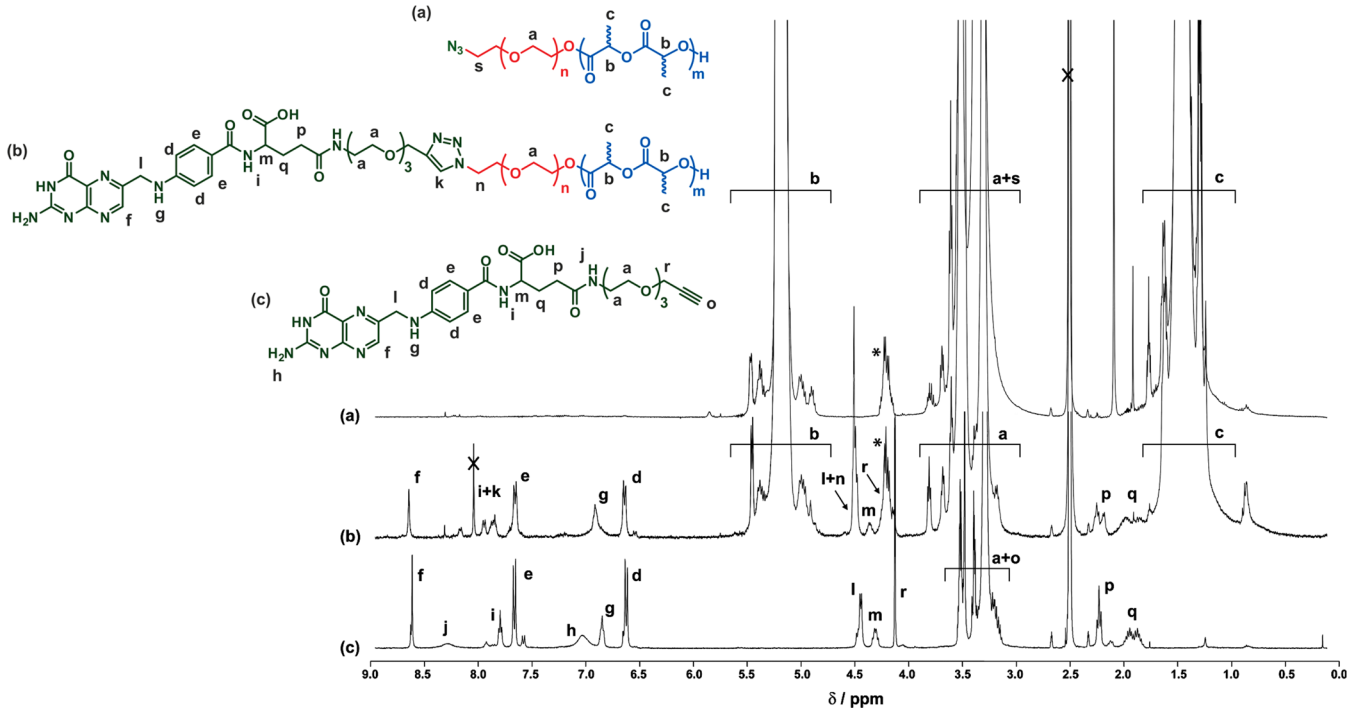

Figure 2. ^{1}H NMR spectra in the 0−9 ppm range in DMSO-d_6 of PLA-*b*-PEG−N_3 (a), PLA-*b*-PEG−FA (b), and alkyne−FA (c). The asterisk indicates the presence of PLA.

receptors (KB-3-1*) was DMEM 2429 (medium without folic acid) in which L-glutamine (200 mM at 0.584 g·L^{-1}) and sodium bicarbonate (3.7 g·L^{-1}) were added. The medium used to culture the KB-3-1 control cell line was the usual DMEM (medium containing 4 mg·L^{-1} folic acid). MCF-7 cells, originating from human breast adenocarcinoma, were obtained from the American Type Culture Collection (ATCC). These cells were cultured in DMEM medium supplemented with 1% penicillin/streptomycin and 10% v/v FBS in a 5% CO_2 humidified atmosphere at 37 °C. This cell line was used as another control, as they do not express folate receptors. PC-3 cells, originating from human prostate adenocarcinoma, were obtained from the Institut Curie. These cells were cultured in RPMI 1640 supplemented with 1% penicillin/streptomycin and 10% FBS in a 5% CO_2 humidified atmosphere at 37 °C. This cell line has been reported to overexpress σ-receptors.[52] Cultures of 85−90% confluency were used for all of the experiments. The cells were trypsinized (trypsin−EDTA), counted, and subcultured into 96-well plates for viability studies as well as into 24-well plates for confocal microscopic studies.

6. Cytotoxicity Assay. In a 96-well plate, 5×10^2 cells dispersed in 50 μL of culture medium (as described above) were deposited per well. After 24 h of preincubation, 50 μL of nanoparticle suspension in PBS at different copolymer concentrations (0.5, 0.1, 0.05, 0.01 mg·mL^{-1}) was added to each well, and the well plates were incubated (5% CO_2, 37 °C) for 48 h. Twenty microliters of a 5 mg·mL^{-1} MTS solution in PBS was added to the wells and then incubated for 3 h. The absorbance of the resulting dye in each well was analyzed at 492 nm wavelength using a microplate reader (Labsystem Multiscan MS, Type 352). The experiments were performed in triplicate. The percentage of the surviving cells was calculated as the absorbance ratio of the treated to the untreated cells.

7. Biological Evaluation of Targeted Nanoparticles. *7.1. Assessment of the Ligand−Receptor Interaction Using Surface Plasmon Resonance (SPR) Spectroscopy.* Interaction of folate-modified nanoparticles was monitored by surface plasmon resonance spectroscopy using a BIAcore T100 (GE Healthcare Life Sciences, Vélizy, France) instrument. For our experiment, series S Sensor chip CM5 (GE Healthcare) was used to immobilize the folate binding protein (FBP) according to a previously described protocol.[53] The immobilization protocol, which was performed at a flow rate of 10 μL·min^{-1}, allowed the binding of ∼6.8 ng·mm^{-2} of FBP per channel. The first flow channel (Fc1) was blocked only by ethanolamine, so that it could be used as a reference channel in order to check whether the dextran is playing a role in the nonspecific adsorption of nanoparticles. The adsorption of PLA-*b*-PEG−FA nanoparticles (5 mg·mL^{-1}) onto the immobilized FBP was assessed and compared with that of the nonfunctionalized PLA-*b*-PEG−OMe nanoparticles as control. All the experiments were conducted at a flow rate of 5 μL·min^{-1} with a contact time of 500 s.

Interaction of biotinylated nanoparticles was monitored using a BIAcore 2000 (GE Healthcare, Uppsala, Sweden). In order to be able to regenerate the sensor chip, a biotin CAPture kit purchased from GE Healthcare was used to study the biotin/streptavidin interaction. The chip coating was made of a carboxymethylated dextran matrix, preimmobilized with a single-strand DNA molecule. Then a biotin CAPture reagent, made of the complementary single-strand DNA molecule conjugated to streptavidin, was used to capture the biotinylated nanoparticles. Concretely, the chip was rehydrated with the running buffer [HEPES-buffered saline−NaCl (HBS-N), GE Healthcare] overnight prior to use. Then the chip surface was conditioned with three 1-min injections of regeneration buffer (6 M guanidine-HCl, 0.25 M NaOH provided within the kit by GE Healthcare) with a flow rate of 10 μL·min^{-1}. The coupling process was performed as follows: (i) biotin CAPture reagent was injected for 5 min at 2 μL·min^{-1} and (ii) the biotinylated nanoparticles (0.0125 mg·mL^{-1}) were then injected for 3 min at 30 μL·min^{-1} and rinsing buffer injection was performed for 3 min. The capture level of nanoparticle was monitored; (iii) finally, the sensor chip surface was regenerated with two injections of 20 s at 5 μL·min^{-1} of the regeneration solution before a new experimental cycle. The analyses were done using BIAevaluation software, version 4.1.1 (GE Healthcare).

7.2. Assessment of Nanoparticle Uptake Using Fluorescence-Activated Cell Sorting (FACS). Uptake of the targeted nanoparticles by the cells has been assessed by flow cytometry. Nanoparticles containing the fluorescent probe FP547 but without folic acid (**N12**; see Table 1) as a control or with folic acid (**N11**; see Table 1) have been prepared using 1% w/v Pluronic F68 as a stabilizer. The KB-3-1 cell line was cultured in folic acid containing medium to facilitate the overexpression of folate receptors (as mentioned previously) in a

dx.doi.org/10.1021/cm403822w | *Chem. Mater.* 2014, 26, 1834−1847

24-well plate up to near confluence (~300 000 cells/well). The culture medium in the wells was replaced with 1 mL of the medium containing nanoparticles, at a final copolymer concentration of ~60 $\mu g \cdot mL^{-1}$, and incubated for different time intervals (from 10 min to 24 h). Afterward, the culture medium was removed, and the cells were washed twice with PBS (1 mL) and subsequently isolated by trypsinization and centrifugation (5 min at 1000*g*). The cell pellet was resuspended in PBS (1 mL), centrifuged (5 min at 1000*g*), and finally fixed by

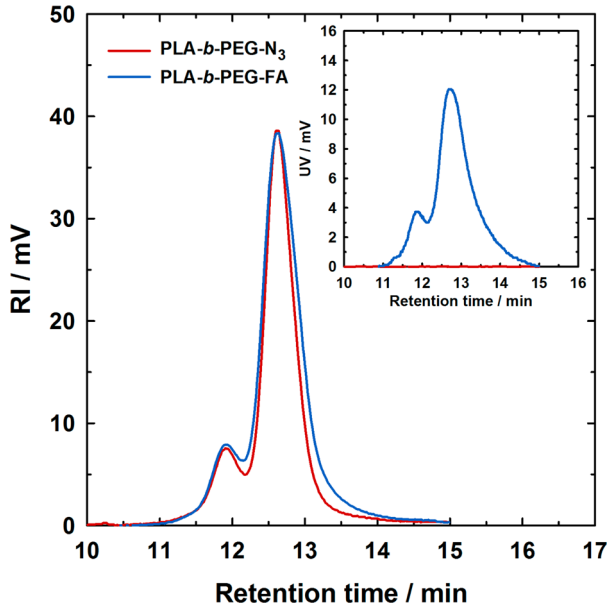

Figure 3. Size exclusion chromatograms of PLA-*b*-PEG−N_3 and PLA-*b*-PEG−FA by DRI (main graphic) and UV detection at 350 nm (inset).

Table 1. Composition and Colloidal Characteristics of Multifunctional PLA-*b*-PEG Nanoparticles

	PLA-*b*-PEG−X[a] (mol %[b])							
expt	OMe	FA	Am	FP547	VB7	av diam[c] (nm)	PSD[c]	zeta potential (mV)
N1	97			1		103	0.15	−12.9
N2	81	16		1		104	0.18	−15.8
N3	71		17	1		116	0.17	−8.4
N4	68	24				118	0.23	−21.7
N5	69	31				116	0.23	−21.2
N6	73	20				112	0.20	−19.6
N7	79	16				106	0.18	−19.0
N8	84	12				111	0.17	−16.6
N9	89	8				109	0.14	−18.0
N10	100					111	0.16	−9.6
N11	69	17		3		110	0.19	−17.3
N12	86			3		109	0.19	−11.6
N13	47		28	2		104	0.13	−10.1
N14	91			2		107	0.14	−7.8
N15	94				5	72	0.16	−17.8
N16	88				9	74	0.19	−23.1
N17	75				19	79	0.26	−15.5
N18	50				38	74	0.21	−25.2
N19	25				57	66	0.20	−33.6
N20	0				76	64	0.15	−35.1

[a]Nature of the copolymers: OMe = methoxy (**C1**), FA = folic acid (**C3**), Am = anisamide (**C4**), FP547 = FP547 fluorescent dye (**C5**), VB7 = biotin (**C8**). [b]Molar fraction of X in the blend determined by ^{1}H NMR. Note that the total percentages, except for that of **N10**, are not 100% due to nonquantitatve coupling for PLA-*b*-PEG−X. [c]Determined by DLS (see Experimental Section).

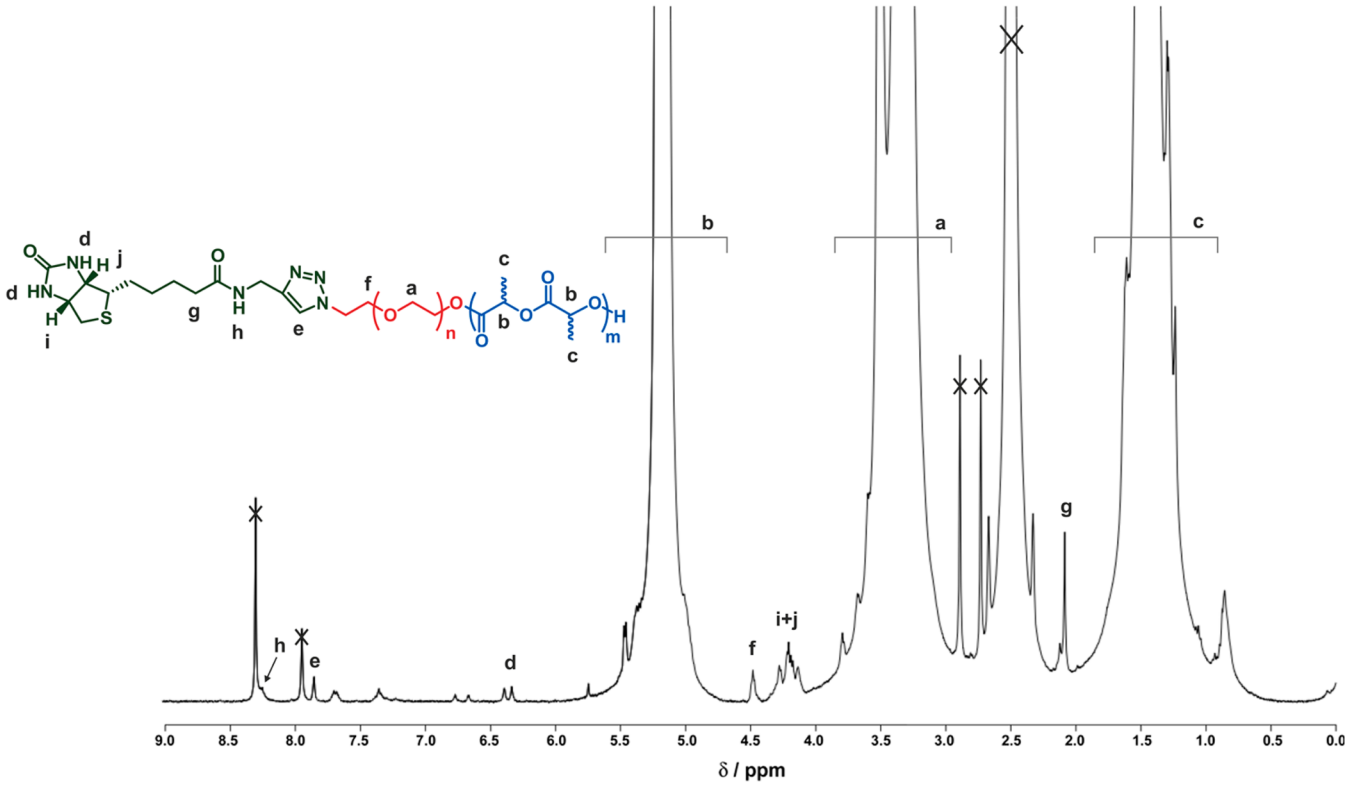

Figure 4. ^{1}H NMR spectra in the 0−9 ppm range in DMSO-d_6 of PLA-*b*-PEG−VB7.

dx.doi.org/10.1021/cm403822w | *Chem. Mater.* 2014, 26, 1834−1847

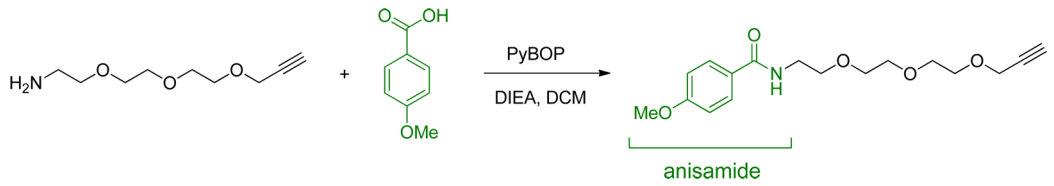

Figure 5. Synthesis of anisamide−tri(ethylene glycol)−alkyne (Am−TEG−alkyne).

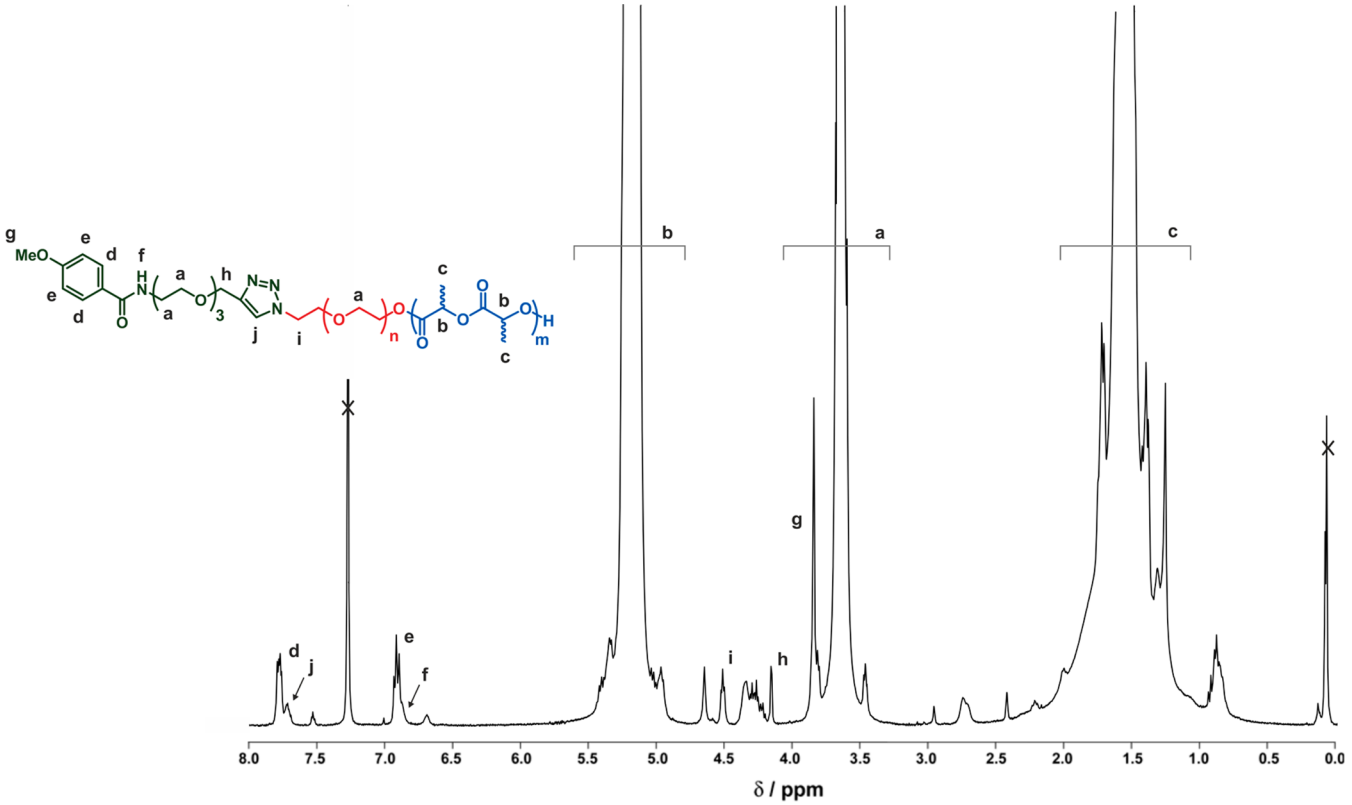

Figure 6. ^{1}H NMR spectrum in the 0−8 ppm range of PLA-*b*-PEG−Am in DMSO-d_6.

incubating in 1% w/v paraformaldehyde in PBS. Flow cytometry analysis of the cell suspensions was carried out using a BD LSRFortessa cell analyzer with an excitation wavelength of 561 nm and an emission signal retrieved between 575 and 589 nm. The same experiment was also performed on PC-3 cells with nanoparticles **N13** and **N14** (Table 1).

7.3. Confocal Microscopy. In vitro imaging of the nanoparticle uptake without or with anisamide as targeting ligand into PC-3 human prostate adenocarcinoma cells overexpressing σ-receptors was performed using confocal microscopy. Nanoparticles containing the fluorescent probe FP547 but without anisamide (**N14**; see Table 1) as a control or with anisamide (**N13**; see Table 1) have been prepared using 1% w/v Pluronic F68 as a stabilizer. Briefly, PC-3 cells were seeded on a type-I collagen-coated glass disk (25 mm in diameter) at a concentration of 25 000 cells·cm^{-2} (or 50 000 cells/mL/well) in a 24-well plate. After 24 h of preincubation, the cells were incubated with an aqueous suspension of nanoparticles (200 μg·mL^{-1}, diluted in RPMI 1640). At 1, 6, and 10 h postincubation, the cells monolayers were washed with fresh medium and then imaged using a confocal laser scanning microscope (LSM 510 META (Zeiss) equipped with a 1 mW helium neon laser and a Plan-Apochromat 63× objective lens (numerical aperture/1.4, oil immersion). Prior to the imaging, the glass disks were submerged into a freshly prepared paraformaldehyde solution (4%) for 10 min. The latter was then neutralized by the addition of ammonium chloride (50 mM for 10 min), and finally, the glass disks were washed three times with PBS. The glass disks were mounted on a glass slide using Vectashield (Vector Laboratories) and fixed with nail varnish. The glass slides were kept in the dark at 4 °C prior to observation. The fluorescence measurements were performed with a long-pass 560 nm emission filter under 543 nm wavelength excitation. To specifically observe the intracellular nanoparticles localization, acquisitions were made at the median plane of the cell monolayer. The pinhole size was set at 1.0 Airy unit (106 μm diameter), giving an optical section thickness of 0.8 μm. Each sample was observed with a zoom factor of 1.5, a master gain of 757, a digital gain of 1, and a digital offset of 0.05. Prior to observations, the autofluorescence of PC-3 cells was checked under the acquisition settings.

RESULTS AND DISCUSSION

1. Synthesis and Characterization of PLA-*b*-PEG−Ligand. In order to ensure an efficient ligand display at the surface of the nanoparticles, the strategy was to prepare amphiphilic block copolymers comprising a biodegradable PLA block to which is attached a linear PEG chain bearing a terminal azide group for further click reaction. Performing the coupling on the PLA-*b*-PEG−N_3 (**C2**) copolymer, prior to the formation of nanoparticles, allows one to well-characterize the resulting conjugate. Importantly, its blending with nonfunctionalized PLA-*b*-PEG (**C1**) and/or PLA-*b*-PEG functionalized with other ligands can conduct to multifunctional PLA-*b*-PEG nanoparticles with tunable surface functionalization, which is of high

dx.doi.org/10.1021/cm403822w | *Chem. Mater.* 2014, 26, 1834−1847

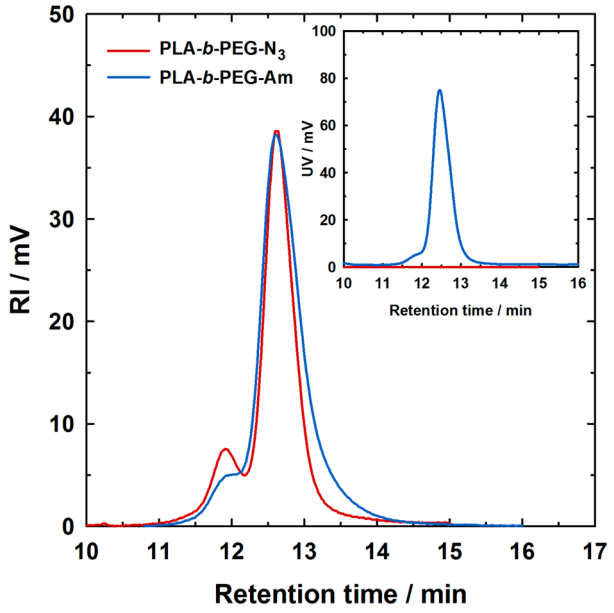

Figure 7. Size exclusion chromatograms of PLA-*b*-PEG−N_3 and PLA-*b*-PEG−Am by DRI (main graphic) and UV detection at 375 nm (inset).

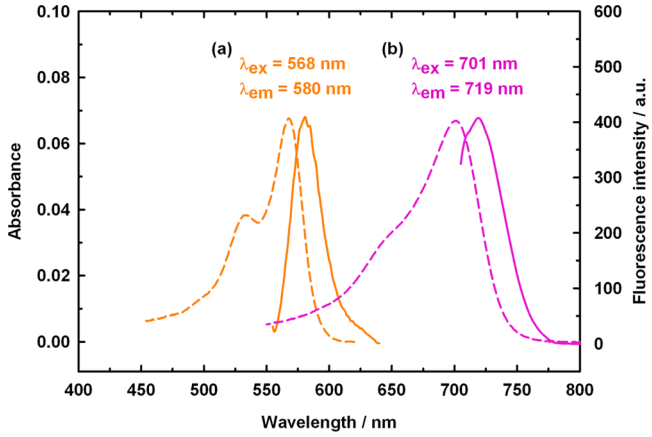

Figure 8. Emission (solid line) and excitation (dashed line) spectra of PLA-*b*-PEG−FP547 (a) and PLA-*b*-PEG−FP682 (b) copolymer.

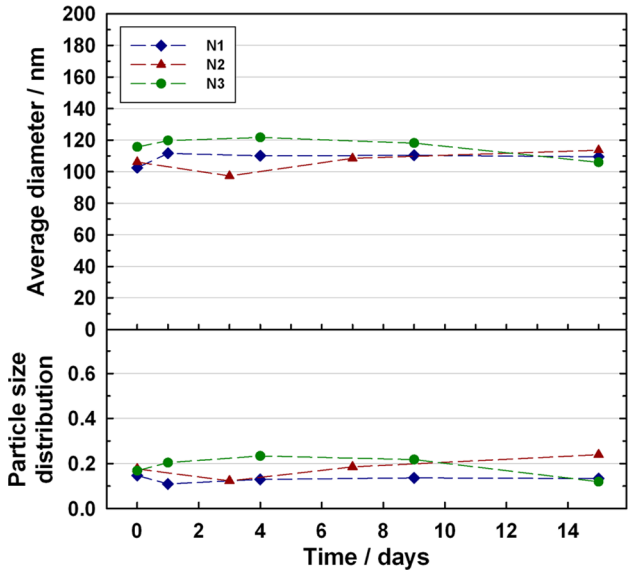

Figure 9. Evolution of the average diameters and the particle size distributions of nanoparticles **N1**−**N3** (Table 1) in PBS stored at 4 °C.

importance for the rational design of efficient drug delivery systems. Noteworthy is the fact that PLA-*b*-PEG (**C1**) was obtained from a 2100 g·mol^{-1} PEG, whereas all functionalized PLA-*b*-PEG−ligands were synthesized with a PEG of 2500 g·mol^{-1} in order to promote the ligand display at the surface of the nanoparticles.

Azidopoly(ethylene glycol) (N_3−PEG−OH) was first obtained from commercially available benzylpoly(ethylene glycol) and used as macroinitiator for the ring-opening polymerization (ROP) of D,L-lactide to furnish well-defined PLA-*b*-PEG−N_3 (**C2**, $M_{n,NMR}$ = 29 200 g·mol^{-1}, $M_{n,SEC}$ = 20100 g·mol^{-1}, $Đ$ = 1.11). Biologically active ligands and fluorescent probes were then derivatized with alkyne moieties and clicked with PLA-*b*-PEG−N_3 under CuAAC conditions. The orthogonality of CuAAC, in combination with the robustness of the PLA-*b*-PEG nanoparticulate system, make this synthetic pathway virtually applicable to any kind of small- to average-sized biologically active ligand and fluorescent probe for the design of multifunctional, biodegradable, and PEGylated nanoparticles. This synthetic flexibility was demonstrated by the use of a variety of ligands, either for targeting cancer cells or for imaging purposes.

The first selected targeting ligands were two vitamins, namely FA and VB7, which are reported to be overexpressed at the surface of a variety of cancer cells.[47,54] For the synthesis of folic acid-containing construct, FA was modified by an alkyne−amino tri(ethylene glycol) linker via EDC/NHS coupling chemistry and subsequently clicked to PLA-*b*-PEG−N_3 (see Experimental Section), followed by an extensive purification to yield the γ-isomer of alkyne−FA, which is considered to be the more active form of FA.[50,51] Successful syntheses of alkyne−FA and PLA-*b*-PEG−FA ($M_{n,NMR}$ = 30 700 g·mol^{-1}, $M_{n,SEC}$ = 19 500 g·mol^{-1}, $Đ$ = 1.16) were confirmed by ^{1}H NMR spectroscopy (Figure 2). All the peaks corresponding to alkyne−FA were assigned, among which were the alkyne proton at 2.5 ppm and the CH_2 in the α-position of the alkyne at 4.1 ppm (Figure 2c). For the purified PLA-*b*-PEG−FA, all the characteristic signals of FA and PLA-*b*-PEG were retrieved in the spectrum, as well as a signal at δ 7.9 ppm (partially overlaid), which is likely to be assigned to the triazole proton resulting from the click chemistry (Figure 2b). On the basis of the peaks at 6.65, 7.65, and 8.65 ppm, a coupling yield of 76% has been calculated.

From SEC analysis using differential refractive index (DRI) and UV (at 350 nm to follow FA) detections, it was observed that the clicked copolymer exhibited a strong UV absorbance that matched with the DRI signal, in contrast to the starting PLA-*b*-PEG−N_3 copolymer, for which no signal was detected (Figure 3). This data, in addition to that revealed by ^{1}H NMR analysis, confirmed the conjugation of FA to the copolymer.

PLA-*b*-PEG−VB7 (**C7**) was successfully synthesized under similar CuAAC conditions from VB7 previously derivatized with propargyl amine (Figure 4). ^{1}H NMR analysis revealed all characteristic signals of the VB7 moiety together with the triazole proton at δ 7.86 ppm and the CH_2 in the α-position of the triazole at δ 4.48 ppm, from which a coupling yield of 52% has been calculated.

For the synthesis of Am-containing construct, the Am moiety was formed in situ during the amidation reaction between *p*-methoxybenzoic acid and the H_2N−TEG−alkyne derivative, leading to the desired Am−TEG−alkyne (Figure 5). ^{1}H NMR

dx.doi.org/10.1021/cm403822w | *Chem. Mater.* 2014, 26, 1834−1847

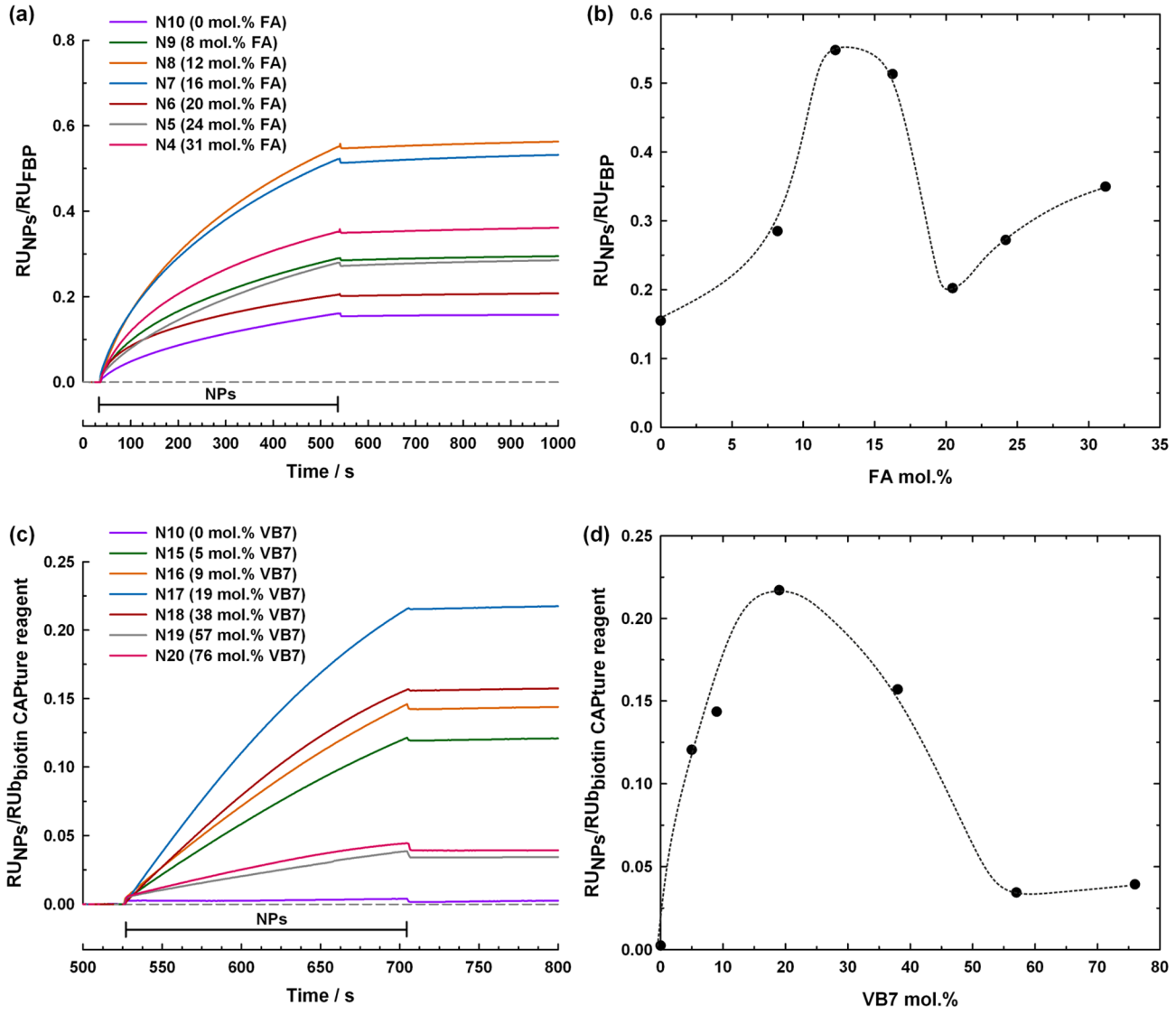

Figure 10. Normalized SPR sensorgrams (RU_{NPs}/RU_{FBP} or $RU_{NPs}/RU_{biotin\ CAPture\ reagent}$) obtained by injections of PLA-*b*-PEG−FA at 5 mg·mL^{-1} (**N4**−**N10**, Table 1) (a) or PLA-*b*-PEG−VB7 at 0.0125 mg·mL^{-1} (**N10**, **N15**−**N20**, Table 1) (c) nanoparticles over folate binding protein (FBP) or streptavidin (SAv), respectively, immobilized on sensor chips. Evolution of the normalized maximum SPR signal as a function of the percentage of FA (b) or VB7 (d) at the surface of the nanoparticles (dashed lines are guides for the eyes).

spectroscopy (Figure 6) revealed all expected proton signals (among which was the triazole proton at δ 7.7 ppm), thus confirming the successful coupling, with a 90% yield.

The SEC profile of PLA-*b*-PEG−Am, with UV detection at 375 nm, which is characteristic of Am (although UV absorbance of the triazole cannot be ruled out at this wavelength), combined with the DRI trace, confirmed the successful linkage of the Am group homogeneously on the polymer chains (Figure 7).

For fluorescence imaging purposes, the fluorescent probes FP547 and FP682 were clicked on PLA-*b*-PEG−N_3. These fluorescent probes were purchased as NHS derivatives, which were subsequently reacted with the H_2N−TEG−alkyne linker. PLA-*b*-PEG−FP547 and PLA-*b*-PEG−FP682 were successfully prepared and characterized by ^{1}H NMR spectroscopy and SEC after extensive purification to remove the unreacted fluorescent probe residues. All characteristic peaks from the fluorescent probes were retrieved in the NMR spectra of the final constructs (see Figure S1, Supporting Information). It is noteworthy to point out that the coupling of the fluorescent probes onto PLA-*b*-PEG−N_3 under CuAAC conditions did not alter their fluorescent properties, as observed from the fluorescence spectra of PLA-*b*-PEG−FP547 and PLA-*b*-PEG−FP682 (Figure 8).

2. Preparation and Characterization of Multifunctional Nanoparticles. Multifunctional nanoparticles containing both a targeting ligand and a fluorescent probe were prepared by the emulsion/solvent evaporation technique. In order to achieve the desired surface ligand and fluorescent probe densities, the different copolymers (i.e., PLA-*b*-PEG−ligand, PLA-*b*-PEG−fluorescent probe, and PLA-*b*-PEG−OMe) were blended at the desired molar ratios. This has been illustrated by the preparation of a large library of a variety of nanoparticles, such as ligand-decorated nanoparticles, fluorescent nanoparticles, and multifunctional nanoparticles decorated with targeting ligands and fluorescent probes (see Table 1).

The nanoparticles were prepared at a concentration of 10 mg·mL^{-1} in PBS and exhibited mean diameters ranging

dx.doi.org/10.1021/cm403822w | *Chem. Mater.* 2014, 26, 1834−1847

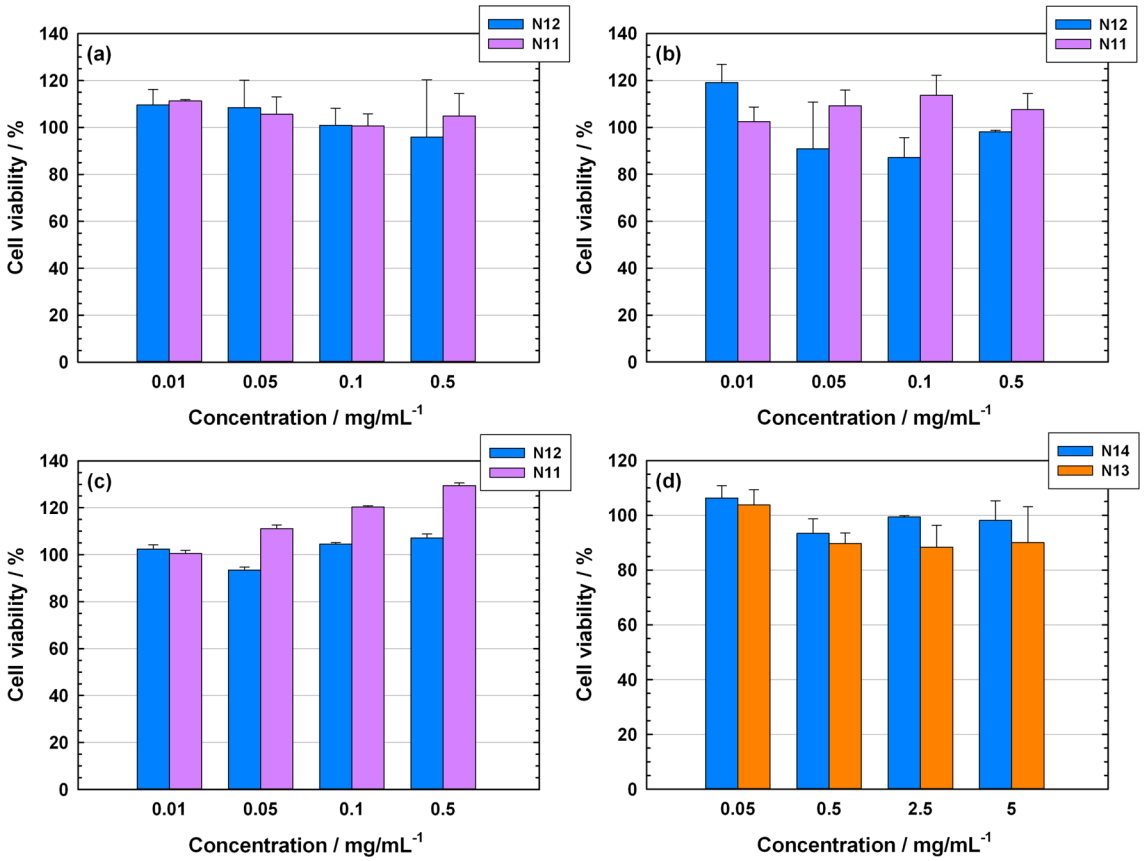

Figure 11. Cell viability (assessed using MTS assay) after a 48 h incubation of KB-3-1 (a), KB-3-1* (b), MCF-7 (c), and PC-3 (d) cells with nonfunctionalized (**N12** and **N14**, Table 1), FA-functionalized (**N11**, Table 1), and Am-functionalized (**N13**, Table 1) nanoparticles, as a function of the nanoparticle concentration. All the experiments were repeated three times, and the results are expressed as the ratio of absorbance of the treated cells (±SD) to that of the untreated control cells.

between 64 and 118 nm (DLS data) with relatively narrow particle size distributions and negative surface charges. TEM experiments were also performed and showed spherical nanoparticles with average diameters in good agreement with DLS measurements (Figure S2, Supporting Information). These nanoparticles exhibited excellent colloidal stability upon storage, as shown with the case of representative fluorescent nanoparticles, without ligands (**N1**) or with ∼16 mol % of either FA (**N2**) or Am (**N3**) ligands, stored for at least 15 days (Figure 9).

4. Assessment of the Recognition of PLA-*b*-PEG−Ligand Nanoparticles by the Corresponding Receptors in Vitro. The ability of the targeting ligands positioned at the distal end of the PEG chains of the nanoparticles to recognize the corresponding receptors was investigated by SPR spectroscopy, which is a mimic of cell surface receptors. SPR analysis was performed for PLA-*b*-PEG−VB7 nanoparticles and PLA-*b*-PEG−FA nanoparticles using streptavidin (SAv)- and folate binding protein (FBP)-coated sensor chips, respectively. The SPR analysis was not performed for PLA-*b*-PEG−Am because σ-receptors are transmembrane proteins that could hardly be coated onto the SPR sensor chips.

To assess the affinity of folic acid from PLA-*b*-PEG−FA nanoparticles toward the folate binding protein, a library of PLA-*b*-PEG−FA nanoparticles was prepared by blending different molar ratios of PLA-*b*-PEG−OMe/PLA-*b*-PEG−FA, leading to FA amounts ranging from 0 to 31 mol % (**N4**−**N10**, Table 1). As expected, the SPR experiments revealed no binding of the nanoparticles of whatever nature with the uncoated sensor chips, whereas strong interactions were observed only between the PLA-*b*-PEG−OMe/PLA-*b*-PEG−FA nanoparticles (**N4**−**N9**) and the FBP-coated sensor chips (Figure 10a), thereby confirming both the suitable positioning of FA on the nanoparticle surface and its ability to specifically recognize the folate receptors. SPR measurements of the nanoparticles prepared with different molar ratios of FA allowed determining the FA concentration needed for optimum binding efficiency of the nanoparticles. Indeed, by plotting the final SPR signal value for each sample as a function of the FA mole percent, the maximum specific binding was found at ∼14 mol % FA (Figure 10b), where the specific signal represented ∼70% of the total signal (the nonspecific signal is roughly estimated by the RU value for the control nanoparticles without FA on their surface, **N10**). Beyond ∼14 mol % FA, the specific signal decreased, suggesting a loss of binding, which is likely due to mild stacking between FA moieties and/or receptor overbinding (i.e., too many FA on the surface of the nanoparticles may facilitate the binding of a single nanoparticle to multiple receptors, thus reducing the number of bonded nanoparticles).[55] In our experiments, the FA content in the nanoparticles could not be increased beyond 31 mol %, due to the limited aqueous solubility of the FA and consequent impact on the colloidal stability of the nanoparticles. Therefore, increasing the local concentration of FA may also result in nonsolvated areas, which would also alter the ligand/receptor recognition. All nanoparticles injected in the reference channel (i.e., dextran functionalized with ethanolamine) resulted in a low binding signal, suggesting that the dextran does

dx.doi.org/10.1021/cm403822w | *Chem. Mater.* 2014, 26, 1834−1847

not induce nanoparticle adsorption. This also supports the idea that the nonspecific signal previously obtained is likely the result of interactions between the PEG chains and the FBP.

Different batches of VB7-functionalized nanoparticles were prepared resulting from copolymer blends of variable PLA-*b*-PEG−OMe/PLA-*b*-PEG−VB7 ratios, with VB7 amounts ranging from 0 to 76 mol % (**N10** and **N15**−**N20**, Table 1). The fine-tuning of the surface-displayed VB7 allowed a dose−response pattern to be obtained. Similarly to the case of FA-functionalized nanoparticles, a maximum of binding of VB7-functionalized nanoparticles to SAv was also noticed, but at ∼20 mol % of VB7. Above this threshold, the binding intensity decreased. This decrease could be attributed again to the hydrophobic interactions between VB7 moieties due to their moderate solubility in water at room temperature and/or receptor overbinding.

Interestingly, at increasing concentration of the VB7-functionalized nanoparticles, the SPR sensorgrams reached a plateau (Figure S3, Supporting Information). This allowed apparent dissociation rate constant ($K_{d,app}$) values of the interaction between biotinylated nanoparticles and SAv to be determined according to the Boltzmann sigmoid method. $K_{d,app}$ ranged from 5×10^{-11} to 5×10^{-10} M (Figure S4, Supporting Information), which is higher than typical biotin/streptavidin K_d values ($\sim 10^{-15}$ M). This could be explained by the two reasons previously mentioned and also by the fact that nanoparticles are spherical systems for which only a small part of the ligands is accessible for receptor recognition.

In summary, the surface functionalization of the nanoparticles with a high ligand density does not guarantee the best ligand−receptor interaction efficiency, and only moderate surface functionalization yields (∼10−20 mol %) may be enough to reach an optimal binding efficacy. Actually, since the tethered ligands interact with protein receptor, it is assumed that the steric hindrance naturally provokes limited ligand−protein accessibility. However, although optimum amounts of FA and VB7 moieties have been clearly shown, these values must be taken with caution, as they have been obtained under specific experimental conditions (e.g., a given receptor density coated on the chip, a given temperature, a given buffer solution), which may not accurately reflects in vitro cell culture or in vivo conditions and therefore may have been subjected to variations.

Interestingly, obtaining a maximum binding/uptake from FA-[56−59] or VB7-decorated[60] nanoparticulate systems has been rarely reported, perhaps because of the difficulty in accurately tuning the amount of surface-exposed ligand. For instance, Poon et al.[56] determined an optimum number of FA moieties at the surface of PEGylated polyester nanoparticles to be ∼2200, which is in excellent agreement with our data (∼2000 FA for **N8** containing 12% FA). Similarly, Bae et al. showed an optimal binding in the ∼10−25% FA range for PEGylated polymeric micelles.[61]

5. Targeting Cancer Cells. Multifunctional nanoparticles (i.e., fluorescent and targeted) were then tested for their ability to target cancer cells in vitro using confocal microscopy and flow cytometry. Fluorescence, which is necessary to track the nanoparticles by each of these techniques, was readily achieved by the addition of a small amount (∼2−3 mol %) of PLA-*b*-PEG−FP547 in the copolymer blends. PC-3 cells, originating from the human prostate adenocarcinoma and exhibiting σ-receptors, were incubated with Am-containing nanoparticles (28 mol % Am, **N13**, Table 1), whereas FA-containing nanoparticles (17 mol % FA, **N11**, Table 1) were tested on both

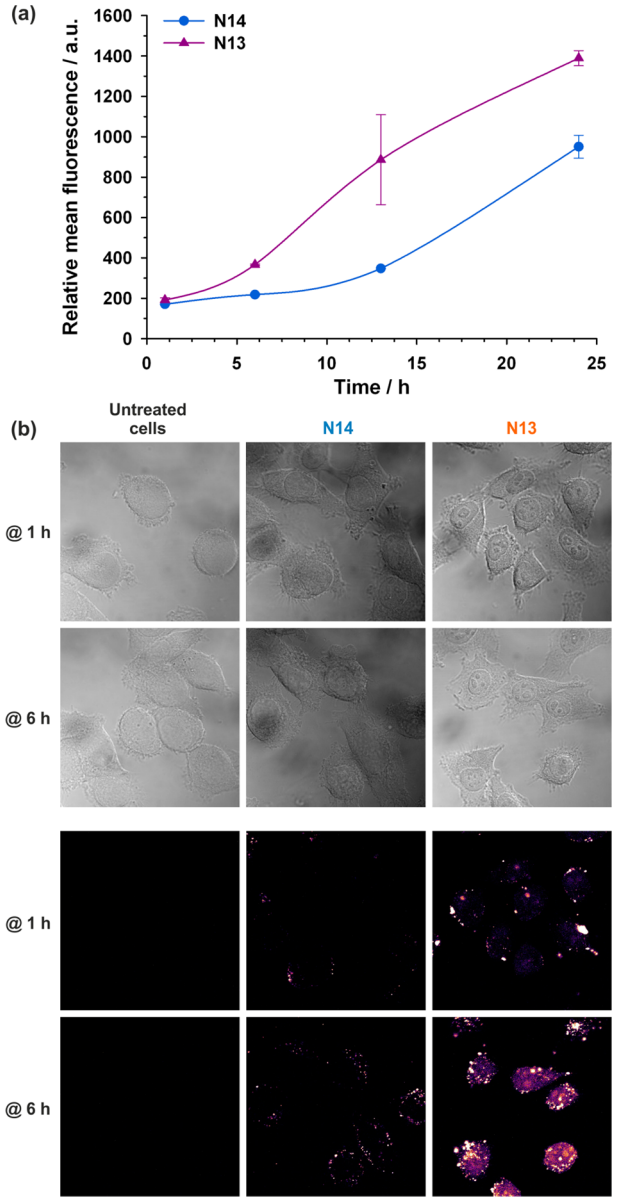

Figure 12. Mean fluorescence intensity evolution with incubation time of PC-3 cells with Am-functionalized nanoparticles **N13** (Table 1) and the nonfunctionalized nanoparticles **N14** (Table 1) (a). Representative Nomarski (top) and confocal microscopy (bottom) images of the PC-3 cells incubated for 1 and 6 h with nonfunctionalized nanoparticles (**N14**, Table 1) and Am-functionalized nanoparticles (**N13**, Table 1) (b). Lines connecting data points are guides for the eye only.

the epidermoid carcinoma cell line KB-3-1, for which folate receptors (FRs) are normally expressed, and its FR overexpressed counterpart KB-3-1* cell line, as well as the MCF-7 breast cancer cell line exhibiting low FR density. In all cases, nonfunctionalized nanoparticles (**N14** and **N12**, Table 1) with identical fluorescence intensity were used as controls. Prior to biological evaluations, the absence of cytotoxicity of each kind of nanoparticles was confirmed by performing MTS assay on each cell line (48 h of incubation with nanoparticles at concentrations up to 0.5 mg·mL^{-1}). MTS assay was used instead of MTT because its absorbance wavelength at 492 nm (570 nm for MTT) does not overlap with the excitation wavelength of the fluorophore FP542. In all cases, whatever the concentration and the nature of the nanoparticles, no noticeable cytotoxicity

dx.doi.org/10.1021/cm403822w | *Chem. Mater.* 2014, 26, 1834−1847

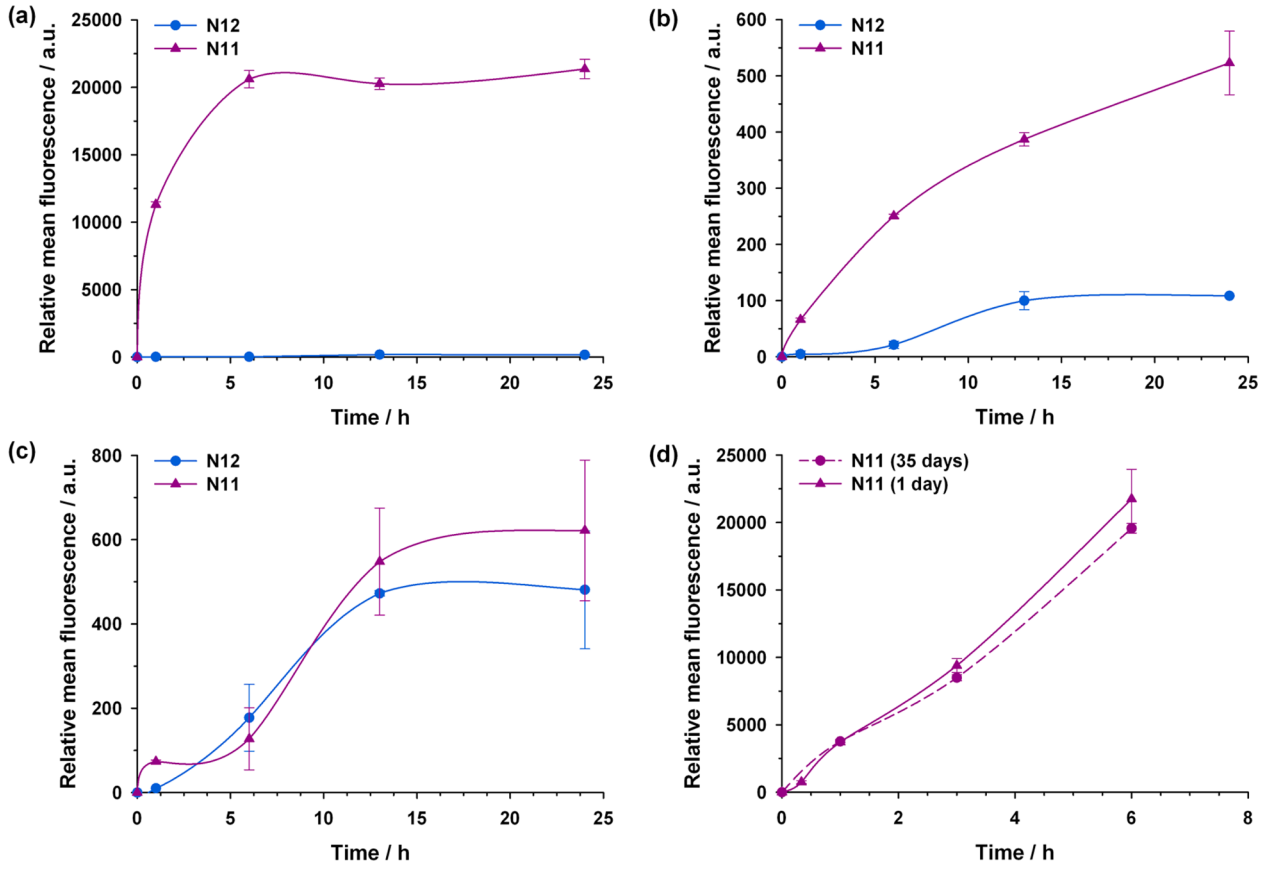

Figure 13. Mean fluorescence intensity evolution with incubation time of KB-3-1* (a), KB-3-1 (b), and MCF-7 (c) cells with FA-functionalized nanoparticles **N11** and the nonfunctionalized nanoparticles **N12** (Table 1). Mean fluorescence evolution with incubation time of KB-3-1* cells (d) with the FA-functionalized nanoparticles **N11** after 1 or 35 days after manufacture. Lines connecting data points are guides for the eye only.

was observed (Figure 11), thus allowing the safe biological evaluations to be performed.

Flow cytometry experiments showed that incubation of PC-3 cells with fluorescent, Am-functionalized nanoparticles **N13** resulted in improved cell uptake from 6 h postincubation compared to that obtained from nonfunctionalized nanoparticles **N14** (Figure 12a). For instance, after 24 h, the uptake of **N13** accounted for an increase of ∼50% compared to that of **N14**. This enhanced uptake was confirmed by confocal microscopy observations, during which PC-3 cells were treated with both kinds of nanoparticles. After 1 h postinjection, **N14** led to a faint fluorescence signal, whereas after 6 h, cells treated with nanoparticles **N13** gave a significantly higher fluorescence signal inside the cells than that obtained with nonfunctionalized nanoparticles (Figure 12b).

In order to assess the FR-mediated targeting, FA-functionalized nanoparticles with 17 mol % FA (**N11**) were incubated with three cancer cell lines (KB-3-1, KB-3-1*, and MCF-7) exhibiting different levels of FR expressions and analyzed by flow cytometry for the measurement of FP547 fluorescence. The results revealed a poor uptake of the nonfunctionalized nanoparticles (**N12**) by all the cell lines tested, while the FA-functionalized nanoparticles showed degrees of binding in good agreement with the levels of FR expression at the surface of the different cell lines (Figure 13). Indeed, both types of nanoparticles (nonfunctionalized nanoparticles and FA-functionalized nanoparticles) were uptaken similarly by the MCF-7 cells, which poorly express FR (Figure 13c). However, FA-functionalized nanoparticles (**N11**) exhibited a ∼5-fold greater cellular uptake than that of the nonfunctionalized nanoparticles (**N12**) in KB-3-1 cells (Figure 13b), while a massive uptake of these nanoparticles by the KB-3-1* cell line overexpressing FR (Figure 13a), which plateaued after 6 h of incubation, has been witnessed and accounted for a ∼115-fold higher cellular uptake as compared to that of the nonfunctionalized nanoparticles over the same period of time.

Another important question that needed to be addressed was the potential surface reorganization of the FA-functionalized nanoparticles with time due to the hydrophobic nature of FA and its possible impact to decrease or even hamper the cell uptake due to buried FA groups inside the hydrophobic nanoparticle core. Uptake of the nanoparticles by KB-3-1* cells was therefore monitored with the FA-functionalized nanoparticles **N11** stored for 35 days and compared with similar nanoparticles freshly prepared. Flow cytometry results revealed no significant difference of the cell uptake between the two kinds of nanoparticles (Figure 13d), thus suggesting the presence of same amount of FA at the surface of nanoparticles even after storage for more than 1 month.

Taken together, these results clearly demonstrated the efficient uptake of targeted Am- functionalized and FA-functionalized nanoparticles into the cancer cells. Thus, the PLA-*b*-PEG−ligand nanoparticles designed using click chemistry were shown to be efficient in cancer cell targeting, and the multifunctional nanoparticles bearing targeting ligand and the fluorescence probe allowed to target cancer cells follow their in vitro fate due to the fluorescent labeling and could simultaneously monitor the response to treatment. This general

dx.doi.org/10.1021/cm403822w | *Chem. Mater.* 2014, 26, 1834−1847

platform is expected to open interesting perspectives for the intracellular delivery of drugs possessing poor cell penetration property.

■ CONCLUSION

In this study, precise macromolecular engineering was performed through a combination of ROP and click chemistry in order to prepare targeted and fluorescently labeled PLA-*b*-PEG nanoparticles for cancer cell targeting and imaging. Well-defined PLA-*b*-PEG−N_3 diblock copolymers were successfully derivatized with a series of (i) biologically active ligands able to recognize cancer cell receptors (i.e., biotin, folic acid, and anisamide) and (ii) fluorescent probes (FP547 and FP682). Multifunctional nanoparticles were then achieved by a simple blending between the different PLA-*b*-PEG copolymers (functional or not) to achieve the desired surface ligand and fluorescent probe densities. Not only were the biologically active ligands efficiently displayed at the surface of the nanoconstructs, as shown by SPR, but their precisely controlled density allowed optimal binding efficiencies to be determined. In vitro cancer cell targeting was successfully demonstrated on different cancer cell lines by flow cytometry and confocal microscopy.

This synthetic strategy, which takes advantage of the orthogonality of the click chemistry coupling, paves the way to the design of various multifunctional PEG-*b*-PLA-based nanoparticles directed toward cancer therapy or against other pathologies, simply by changing the nature of the functional moiety in a Lego-type fashion.

■ ASSOCIATED CONTENT

Ⓢ Supporting Information

^{1}H NMR spectrum of PLA-*b*-PEG−FP547 copolymer, TEM images of the nanoparticles, and characterization of PLA-*b*-PEG−VB7 nanoparticles by SPR. This material is available free of charge via the Internet at http://pubs.acs.org.

■ AUTHOR INFORMATION

Corresponding Author

*E-mail: julien.nicolas@u-psud.fr. Tel: +33 1 46 83 58 53. Fax: +33 1 46 83 55 11.

Notes

The authors declare no competing financial interest.

■ ACKNOWLEDGMENTS

The authors are thankful to Sanofi colleagues Odile Angouillant-Boniface and Dr. Eric Brohan for the preparative HPLC experiments of alkyne−FA, to Danielle Le Métayer for her help with the SPR experiments, to Valérie Nicolas (Plateforme Imagerie Cellulaire, IFR 141) and Sophie Grivès for their help with the confocal microscopy exeriments, and to Dr. Dominique Lesuisse from Sanofi for the postdoc funding of N.H. N.M. is also grateful to Sanofi for financial support. This work has benefited from the facilities and expertise of the platform for Transmission Electron Microscopy of IMAGIF (Centre de recherché de Gif). The CNRS and the French Ministry of Research are also warmly acknowledged for financial support.

■ REFERENCES

(1) Farokhzad, O. C.; Langer, R. *ACS Nano* **2009**, *3*, 16.
(2) Uhrich, K. E.; Cannizzaro, S. M.; Langer, R. S.; Shakesheff, K. M. *Chem. Rev.* **1999**, *99*, 3181.
(3) Peer, D.; Karp, J. M.; Hong, S.; Farokhzad, O. C.; Margalit, R.; Langer, R. *Nat. Nanotechnol.* **2007**, *2*, 751.
(4) Brigger, I.; Dubernet, C.; Couvreur, P. *Adv. Drug Delivery Rev.* **2002**, *54*, 631.
(5) Panyam, J.; Labhasetwar, V. *Adv. Drug Delivery Rev.* **2003**, *55*, 329.
(6) Vauthier, C.; Dubernet, C.; Fattal, E.; Pinto-Alphandary, H.; Couvreur, P. *Adv. Drug Delivery Rev.* **2003**, *55*, 519.
(7) Nicolas, J.; Mura, S.; Brambilla, D.; Mackiewicz, N.; Couvreur, P. *Chem. Soc. Rev.* **2013**, *42*, 1147.
(8) Torchilin, V. P. *Adv. Drug Delivery Rev.* **2012**, *64*, 302.
(9) Sapsford, K. E.; Algar, W. R.; Berti, L.; Gemmill, K. B.; Casey, B. J.; Oh, E.; Stewart, M. H.; Medintz, I. L. *Chem. Rev.* **2013**, *113*, 1904.
(10) Mura, S.; Nicolas, J.; Couvreur, P. *Nat. Mater.* **2013**, *12*, 991.
(11) Elsabahy, M.; Wooley, K. L. *Chem. Soc. Rev.* **2012**, *41*, 2545.
(12) Bazile, D. V.; Ropert, C.; Huve, P.; Verrecchia, T.; Mariard, M.; Frydman, A.; Veillard, M.; Spenlehauer, G. *Biomaterials* **1992**, *13*, 1093.
(13) Cattelan, A. M.; Bauer, U.; Trevenzoli, M.; Sasset, L.; Campostrini, S.; Facchin, C.; Pagiaro, E.; Gerzeli, S.; Cadrobbi, P.; Chiarelli, A. *Arch. Dermatol.* **2006**, *142*, 329.
(14) Hrkach, J.; Von Hoff, D.; Mukkaram Ali, M.; Andrianova, E.; Auer, J.; Campbell, T.; De Witt, D.; Figa, M.; Figueiredo, M.; Horhota, A.; Low, S.; McDonnell, K.; Peeke, E.; Retnarajan, B.; Sabnis, A.; Schnipper, E.; Song, J. J.; Song, Y. H.; Summa, J.; Tompsett, D.; Troiano, G.; Van Geen Hoven, T.; Wright, J.; LoRusso, P.; Kantoff, P. W.; Bander, N. H.; Sweeney, C.; Farokhzad, O. C.; Langer, R.; Zale, S. *Sci. Transl. Med.* **2012**, *4*, 128ra39.
(15) Kolishetti, N.; Dhar, S.; Valencia, P. M.; Lin, L. Q.; Karnik, R.; Lippard, S. J.; Langer, R.; Farokhzad, O. C. *Proc. Natl. Acad. Sci. U. S. A.* **2010**, *107*, 17939.
(16) Farokhzad, O. C.; Jon, S.; Khademhosseini, A.; Tran, T.-N. T.; LaVan, D. A.; Langer, R. *Cancer Res.* **2004**, *64*, 7668.
(17) Chan, J. M.; Zhang, L.; Tong, R.; Ghosh, D.; Gao, W.; Liao, G.; Yuet, K. P.; Gray, D.; Rhee, J.-W.; Cheng, J.; Golomb, G.; Libby, P.; Langer, R.; Farokhzad, O. C. *Proc. Natl. Acad. Sci. U. S. A.* **2010**, *107*, 2213.
(18) Wang, Z. H.; Wang, Z. Y.; Sun, C. S.; Wang, C. Y.; Jiang, T. Y.; Wang, S. L. *Biomaterials* **2010**, *31*, 908.
(19) Goto, M.; Yura, H.; Chang, C.-W.; Kobayashi, A.; Shinoda, T.; Maeda, A.; Kojima, S.; Kobayashi, K.; Akaike, T. *J. Controlled Release* **1994**, *28*, 223.
(20) Yoo, H. S.; Park, T. G. *J. Controlled Release* **2004**, *96*, 273.
(21) Kolb, H. C.; Finn, M. G.; Sharpless, K. B. *Angew. Chem., Int. Ed.* **2001**, *40*, 2004.
(22) Kolb, H. C.; Sharpless, K. B. *Drug Discovery Today* **2003**, *8*, 1128.
(23) Wu, P.; Feldman, A. K.; Nugent, A. K.; Hawker, C. J.; Scheel, A.; Voit, B.; Pyun, J.; Frechet, J. M. J.; Sharpless, K. B.; Fokin, V. V. *Angew. Chem., Int. Ed.* **2004**, *43*, 3928.
(24) Malkoch, M.; Schleicher, K.; Drockenmuller, E.; Hawker, C. J.; Russell, T. P.; Wu, P.; Fokin, V. V. *Macromolecules* **2005**, *38*, 3663.
(25) Mynar, J. L.; Choi, T.-L.; Yoshida, M.; Kim, V.; Hawker, C. J.; Frechet, J. M. J. *Chem. Commun.* **2005**, 5169.
(26) Wang, Q.; Chan, T. R.; Hilgraf, R.; Fokin, V. V.; Sharpless, K. B.; Finn, M. G. *J. Am. Chem. Soc.* **2003**, *125*, 3192.
(27) Parrish, B.; Breitenkamp, R. B.; Emrick, T. *J. Am. Chem. Soc.* **2005**, *127*, 7404.
(28) Hatzakis, N. S.; Engelkamp, H.; Velonia, K.; Hofkens, J.; Christianen, P. C. M.; Svendsen, A.; Patkar, S. A.; Vind, J.; Maan, J. C.; Rowan, A. E.; Nolte, R. J. M. *Chem. Commun.* **2006**, 2012.
(29) Lee, L. V.; Mitchell, M. L.; Huang, S.-J.; Fokin, V. V.; Sharpless, K. B.; Wong, C.-H. *J. Am. Chem. Soc.* **2003**, *125*, 9588.
(30) Manetsch, R.; Krasinski, A.; Radic, Z.; Raushel, J.; Taylor, P.; Sharpless, K. B.; Kolb, H. C. *J. Am. Chem. Soc.* **2004**, *126*, 12809.
(31) Krasinski, A.; Radic, Z.; Manetsch, R.; Raushel, J.; Taylor, P.; Sharpless, K. B.; Kolb, H. C. *J. Am. Chem. Soc.* **2005**, *127*, 6686.
(32) Helms, B.; Mynar, J. L.; Hawker, C. J.; Frechet, J. M. J. *J. Am. Chem. Soc.* **2004**, *126*, 15020.

(33) Opsteen, J. A.; van Hest, J. C. M. *Chem. Commun.* **2005**, 57.
(34) Mantovani, G.; Ladmiral, V.; Tao, L.; Haddleton, D. M. *Chem. Commun.* **2005**, 2089.
(35) Sumerlin, B. S.; Tsarevsky, N. V.; Louche, G.; Lee, R. Y.; Matyjaszewski, K. *Macromolecules* **2005**, *38*, 7540.
(36) Quemener, D.; Davis, T. P.; Barner-Kowollik, C.; Stenzel, M. H. *Chem. Commun.* **2006**, 5051.
(37) Nicolas, J.; Bensaid, F.; Desmaele, D.; Grogna, M.; Detrembleur, C.; Andrieux, K.; Couvreur, P. *Macromolecules* **2008**, *41*, 8418.
(38) Le Droumaguet, B.; Nicolas, J.; Brambilla, D.; Mura, S.; Maksimenko, A.; De Kimpe, L.; Salvati, E.; Zona, C.; Airoldi, C.; Canovi, M.; Gobbi, M.; Noiray, M.; La Ferla, B.; Nicotra, F.; Scheper, W.; Flores, O.; Masserini, M.; Andrieux, K.; Couvreur, P. *ACS Nano* **2012**, *6*, 5866.
(39) Zhang, S.; Chan, K. H.; Prud'homme, R. K.; Link, A. J. *Mol. Pharm.* **2012**, *9*, 2228.
(40) Saeed, A. O.; Magnusson, J. P.; Moradi, E.; Soliman, M.; Wang, W.; Stolnik, S.; Thurecht, K. J.; Howdle, S. M.; Alexander, C. *Bioconjugate Chem.* **2011**, *22*, 156.
(41) Li, X.; Qian, Y.; Liu, T.; Hu, X.; Zhang, G.; You, Y.; Liu, S. *Biomaterials* **2011**, *32*, 6595.
(42) Gref, R.; Minamitake, Y.; Peracchia, M. T.; Trubetskoy, V.; Torchilin, V.; Langer, R. *Science* **1994**, *263*, 1600.
(43) Bazile, D.; Prud'homme, C.; Bassoullet, M.-T.; Marland, M.; Spenlehauer, G.; Veillard, M. *J. Pharm. Sci.* **1995**, *84*, 493.
(44) Bazile, D.; Couvreur, P.; Lakkireddy, H. R.; Mackiewicz, N.; Nicolas, J. Functional PLA-PEG copolymers, the nanoparticles thereof, their preparation and use for targeted drug delivery and imaging. WO2013127949, 2013.
(45) Zhang, Y.; Kim, W. Y.; Huang, L. *Biomaterials* **2013**, *34*, 3447.
(46) Guo, J.; Ogier, J. R.; Desgranges, S.; Darcy, R.; O'Driscoll, C. *Biomaterials* **2012**, *33*, 7775.
(47) Russell-Jones, G.; McTavish, K.; McEwan, J.; Rice, J.; Nowotnik, D. *J. Inorg. Biochem.* **2004**, *98*, 1625.
(48) Stella, B.; Marsaud, V.; Arpicco, S.; Geraud, G.; Cattel, L.; Couvreur, P.; Renoir, J.-M. *J. Drug Targeting* **2007**, *15*, 146.
(49) Wang, X.; Liu, L.; Luo, Y.; Zhao, H. *Langmuir* **2009**, *25*, 744.
(50) Bae, Y.; Jang, W.-D.; Nishiyama, N.; Fukushima, S.; Kataoka, K. *Mol. BioSyst.* **2005**, *1*, 242.
(51) Wang, S.; Lee, R. J.; Mathias, C. J.; Green, M. A.; Low, P. S. *Bioconjugate Chem.* **1996**, *7*, 56.
(52) Megalizzi, V.; Mathieu, V.; Mijatovic, T.; Gailly, P.; Debeir, O.; De Neve, N.; Van Damme, M.; Bontempi, G.; Haibe-Kains, B.; Decaestecker, C.; Kondo, Y.; Kiss, R.; Lefranc, F. *Neoplasia* **2007**, *9*, 358.
(53) Johnsson, B.; Lofas, S.; Lindquist, G. *Anal. Biochem.* **1991**, *198*, 268.
(54) Low, P. S.; Henne, W. A.; Doorneweerd, D. D. *Acc. Chem. Res.* **2008**, *41*, 120.
(55) Saul, J. M.; Annapragada, A.; Natarajan, J. V.; Bellamkonda, R. V. *J. Controlled Release* **2003**, *92*, 49.
(56) Poon, Z.; Chen, S.; Engler, A. C.; Lee, H.-i.; Atas, E.; von Maltzahn, G.; Bhatia, S. N.; Hammond, P. T. *Angew. Chem., Int. Ed.* **2010**, *49*, 7266.
(57) Nukolova, N. V.; Oberoi, H. S.; Cohen, S. M.; Kabanov, A. V.; Bronich, T. K. *Biomaterials* **2011**, *32*, 5417.
(58) Saha, A.; Basiruddin, S. K.; Maity, A. R.; Jana, N. R. *Langmuir* **2013**, *29*, 13917.
(59) Zhao, H.; Yung, L. Y. L. *Int. J. Pharm.* **2008**, *349*, 256.
(60) Qi, K.; Ma, Q.; Remsen, E. E.; Clark, C. G., Jr.; Wooley, K. L. *J. Am. Chem. Soc.* **2004**, *126*, 6599.
(61) Bae, Y.; Nishiyama, N.; Kataoka, K. *Bioconjugate Chem.* **2007**, *18*, 1131.